2

Eulerian and Lagrangian Fundamentals

Classical continuum mechanics focuses on the deformation field of moving continua. This deformation field is composed of the trajectories of all material elements, labeled by their initial positions. This initial-condition-based, material description is what we mean here by the *Lagrangian description* of fluid motion (see Fig. 2.1).

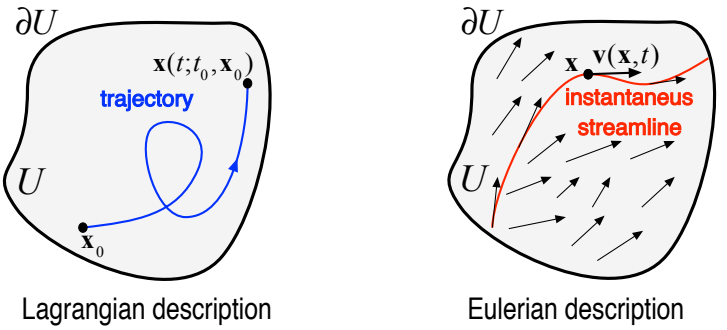

Figure 2.1 Lagrangian (trajectory-based) and Eulerian (velocity-field-based) descriptions of fluid flow.

In contrast to typical solid-body deformations, however, fluid deformation may be orders of magnitude larger than the net displacement of the total fluid mass. For example, the center of mass of a turbulent, incompressible fluid in a closed tank experiences no displacement in the lab frame, yet individual fluid elements undergo deformations that no material used in structural engineering would withstand. The difficulty of tracking individual fluid elements has traditionally shifted the focus in fluid mechanics from individual trajectories to the instantaneous velocity field and quantities derived from the velocity field, such as the vorticity and momentum. We refer here to the instantaneous-position-based approach to continuum motion as the *Eulerian description* (see Fig. 2.1).

Our discussion of the Eulerian view of fluids will be substantially shorter than usual in fluids textbooks, mainly because the focus here is on flow kinematics rather than the governing equations of fluids. Indeed, all transport barriers and coherent structures to be discussed in this book can be defined and located purely from available velocity data. The only conceptual exceptions to this rule are barriers to the transport of dynamically active quantities (see Chapter 9), whose identification depends on the constitutive equation of the fluid. Once this dependence is clarified, however, the active barriers can still be identified from operations performed solely on the velocity field.

https://doi.org/10.1017/9781009225199.003 Published online by Cambridge University Press

In contrast, our review of Lagrangian aspects of fluid mechanics in this chapter will be more extensive than customary in fluid mechanics textbooks, including those fully dedicated to Lagrangian fluid dynamics (such as Bennett, 2006). This is because our analysis of material barriers to transport will rely extensively on tools from dynamical systems theory and continuum mechanics that are not traditionally part of the toolkit of fluid mechanics.

2.1 Eulerian Description of Fluid Motion

We refer to scalar, vector and tensor fields defined over spatial positions $\mathbf{x} \in U \subset \mathbb{R}^n$ as *Eulerian quantities*. The bounded spatial domain U will be either two-dimensional (2D) for $n = 2$ or three-dimensional (3D) for $n = 3$. Unless otherwise noted, we will always assume that these fields are known for times t ranging over a finite time interval $[t_1, t_2]$.

The central Eulerian quantity in descriptions of flow evolution is the velocity field $\mathbf{v}(\mathbf{x}, t)$, which we call *steady* if it is constant in time (i.e., of the form $\mathbf{v}(\mathbf{x})$). When the velocity field does depend on time explicitly, we call it *unsteady*.

2.1.1 Eulerian Scalars, Vector Fields and Tensors

A scalar field defined at all positions $\mathbf{x}$ and times t is an *Eulerian scalar* field. For instance, any evolving tracer concentration field $c(\mathbf{x}, t)$ is an Eulerian scalar field.

An *Eulerian vector field* is a time-dependent vector field $\mathbf{u}(\mathbf{x}, t)$ defined on the domain U. The velocity field $\mathbf{v}(\mathbf{x}, t)$ of a moving fluid as well as its vorticity $\boldsymbol{\omega}(\mathbf{x}, t) = \boldsymbol{\nabla} \times \mathbf{v}(\mathbf{x}, t)$ are examples of Eulerian vector fields. In contrast, an eigenvector field $\mathbf{e}_i(x, t)$ of an Eulerian tensor field (to be defined below) is, in general, *not* an Eulerian vector field because it has no well-defined length or orientation. Accordingly, we refer to such eigenvector fields as *Eulerian direction fields*.

An *Eulerian tensor field* $\mathbf{A}(\mathbf{x}, t)$ is a linear mapping family that maps each tangent space $T_{\mathbf{x}}\mathbb{R}^n$ (see Appendix A.4) into itself at all positions $\mathbf{x} \in U$ for all times $t \in [t_1, t_2]$. Examples include the *velocity gradient tensor* $\boldsymbol{\nabla}\mathbf{v}(\mathbf{x}, t)$, the symmetric *rate-of-strain tensor* $\mathbf{S}(\mathbf{x}, t)$ and the skew-symmetric *spin tensor* $\boldsymbol{W}(\mathbf{x}, t)$, with the latter two defined as

$$\mathbf{S} = \frac{1}{2}\Big[\boldsymbol{\nabla}\mathbf{v} + (\boldsymbol{\nabla}\mathbf{v})^{\mathrm{T}}\Big], \quad \mathbf{W} = \frac{1}{2}\Big[\boldsymbol{\nabla}\mathbf{v} - (\boldsymbol{\nabla}\mathbf{v})^{\mathrm{T}}\Big]. \tag{2.1}$$

Here and going forward, the superscript T will refer to transposition. An important relationship between the spin tensor and the vorticity vector is

$$\mathbf{We} = \frac{1}{2}\boldsymbol{\omega}\times\mathbf{e} \tag{2.2}$$

for all vectors $\mathbf{e} \in \mathbb{R}^3$ (see Appendix A.12). In other words, the vector associated with the spin tensor is half of the vorticity vector.

Passive Eulerian scalar, vector and *tensor fields* are field quantities whose evolution has no impact on the underlying velocity field $\mathbf{v}$. Examples of such fields include a dye concentration field $c(\mathbf{x}, t)$, its gradient vector field $\boldsymbol{\nabla} c(\mathbf{x}, t)$ and its Hessian tensor field $\boldsymbol{\nabla}^2 c(\mathbf{x}, t)$. In contrast, *active Eulerian fields*, such as the velocity norm $|\mathbf{v}(\mathbf{x}, t)|$, the vorticity vector $\boldsymbol{\omega}(\mathbf{x}, t)$ and the rate-of-strain tensor $\mathbf{S}(\mathbf{x}, t)$, are fields whose evolution directly impacts the velocity field.

https://doi.org/10.1017/9781009225199.003 Published online by Cambridge University Press

2.1.2 Streamlines and Stagnation Points in 2D Flows

A parametrized curve that is everywhere tangent to the velocity field $\mathbf{v}(\mathbf{x},t)$ at time t is called an instantaneous *streamline*, as shown in Fig. 2.1. Any streamline $\mathbf{x}(s;t)$, parametrized by $s \in \mathbb{R}$ at time t, is therefore composed of solutions of the autonomous ordinary differential equation (ODE)

$$\mathbf{x}' = \mathbf{v}(\mathbf{x},t), \tag{2.3}$$

in which the prime denotes differentiation with respect to s and t plays the role of a parameter. We call the flow *incompressible* if $\mathbf{v}$ is divergence-free (or *solenoidal*), i.e., $\nabla \cdot \mathbf{v} \equiv 0$.

For 2D incompressible flows, there exists a *stream function* $\psi(\mathbf{x},t)$ such that the velocity field can be written as

$$\mathbf{v}(\mathbf{x},t) = \mathbf{J}\nabla\psi(\mathbf{x},t), \qquad \mathbf{J} = \begin{pmatrix} 0 & 1 \\ -1 & 0 \end{pmatrix}. \tag{2.4}$$

At any time instant t, streamlines are contained in the level curves (or isocontours) of $\psi(\mathbf{x},t)$, given that

$$\frac{d}{ds}\psi(\mathbf{x}(s),t) = \nabla\psi(\mathbf{x}(s),t)\cdot\mathbf{v}(\mathbf{x}(s),t) = \langle\nabla\psi(\mathbf{x}(s),t),\mathbf{J}\nabla\psi(\mathbf{x}(s),t)\rangle \equiv 0 \tag{2.5}$$

holds by the skew-symmetry of the matrix $\mathbf{J}$. Equation (2.4) says that the stream function $\nabla\psi(\mathbf{x},t)$ acts as a Hamiltonian function for 2D incompressible fluid particle motion (see Appendix A.5 for more on Hamiltonian systems). We note that in 3D flows, no scalar stream function is guaranteed to exist from which the full velocity field could be derived.

An *instantaneous stagnation point* is a time-dependent point $\mathbf{p}(t)$ at which the velocity field $\mathbf{v}$ vanishes at time t, i.e.,

$$\mathbf{v}(\mathbf{p}(t),t) = \mathbf{J}\nabla\psi(\mathbf{p}(t),t) = \mathbf{0}. \tag{2.6}$$

At such points, the linearization

$$\boldsymbol{\xi}' = \nabla\mathbf{v}(\mathbf{p}(t),t)\boldsymbol{\xi} = \mathbf{J}\nabla^2\psi(\mathbf{p}(t),t)\boldsymbol{\xi}, \qquad \boldsymbol{\xi} \in \mathbb{R}^2 \tag{2.7}$$

of the differential equation (2.3) determines the instantaneous local streamline geometry, which depends on the eigenvalues and eigenvectors of $\nabla\mathbf{v}(\mathbf{p}(t),t)$. The eigenvalues of the velocity gradient satisfy the characteristic equation

$$\lambda^2 - (\nabla\cdot\mathbf{v})\,\lambda + \det\nabla\mathbf{v} = 0. \tag{2.8}$$

This equation simplifies to

$$\lambda^2 + \det\nabla\mathbf{v} = 0 \tag{2.9}$$

for incompressible flows, yielding the two eigenvalues of $\nabla\mathbf{v}(\mathbf{p}(t),t)$ in the form

$$\lambda_{1,2}(t) = \pm\sqrt{-\det\nabla\mathbf{v}(\mathbf{p}(t),t)}. \tag{2.10}$$

Figure 2.2 shows the possible local streamline geometries for different $\lambda_{1,2}$ configurations: *hyperbolic* (saddle-type) *stagnation point*; *elliptic* (center-type) *stagnation point*; *nondegenerate parabolic stagnation point* (local shear flow arising near a stagnation point on a free-slip boundary); *degenerate parabolic stagnation point* (locally quiescent flow arising near a point on a no-slip boundary). At nondegenerate parabolic stagnation points,

https://doi.org/10.1017/9781009225199.003 Published online by Cambridge University Press

only one independent eigenvector exists. At degenerate parabolic stagnation points, any vector is an eigenvector. Importantly, these instantaneous streamline geometries only give an accurate description of fluid particle motion if the velocity field is steady. In unsteady flows, the fluid motion can differ vastly from the local streamline geometry, as we shall see throughout §2.2.

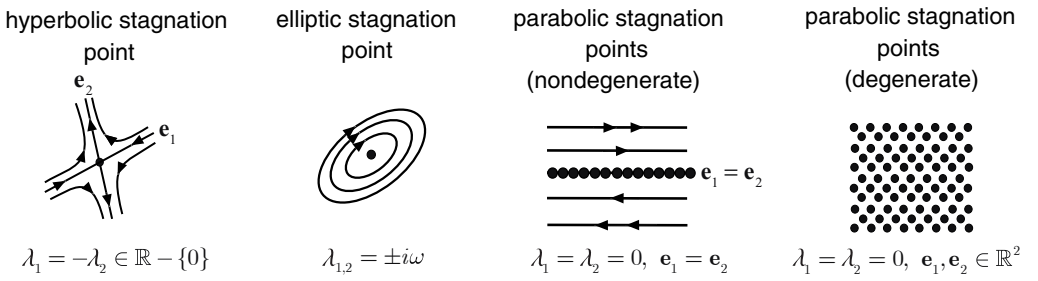

Figure 2.2 The four possible linearized streamline geometries at an instantaneous stagnation point of a 2D incompressible flow. The eigenvalues of $\nabla \mathbf{v}(\mathbf{p}(t), t)$ are λ_1 and λ_2, with corresponding real eigenvectors $\mathbf{e}_1$ and $\mathbf{e}_2$, whenever $\lambda_{1,2}$ are real numbers.

Instantaneous flow patterns in the velocity field of a 2D flow are separated from each other by special streamlines, or *separatrices*, across which there is a change in the topology of streamlines. By the implicit function theorem (see Appendix A.1), such a change in the streamline geometry can only occur near points where the gradient $\nabla \psi(\mathbf{x}, t)$ vanishes. We then conclude by Eq. (2.6) that separatrices between different streamline patterns must necessarily be streamlines that contain at least one stagnation point. With the exception of elliptic stagnation points, all other types of stagnation points shown in Fig. 2.2 can be contained in a streamline. Accordingly, the possible separatrices in 2D incompressible flows are shown in Fig. 2.3.

Of these, *homoclinic streamlines* connecting hyperbolic stagnation points to themselves and *heteroclinic streamlines* connecting two hyperbolic or nondegenerate parabolic stagnation points on a boundary to each other are *structurally stable*, i.e., smoothly persist under small perturbations of the stream function (see §2.2.7 for a more formal definition of structural stability). Indeed, the endpoints of these connecting streamlines are forced to be on the same level set of the stream function even after small perturbations, as illustrated in Fig. 2.4 (left).

In contrast, heteroclinic streamlines connecting two points away from boundaries or an off-boundary point to an on-boundary point are structurally unstable. Indeed, in the absence of any symmetry that would force the endpoints of such a connection to remain on the same level set of the stream function, small perturbations to the stream function will generally cause the two stagnation points to move to different level curves of the stream function (see Fig. 2.4 (right)).

https://doi.org/10.1017/9781009225199.003 Published online by Cambridge University Press

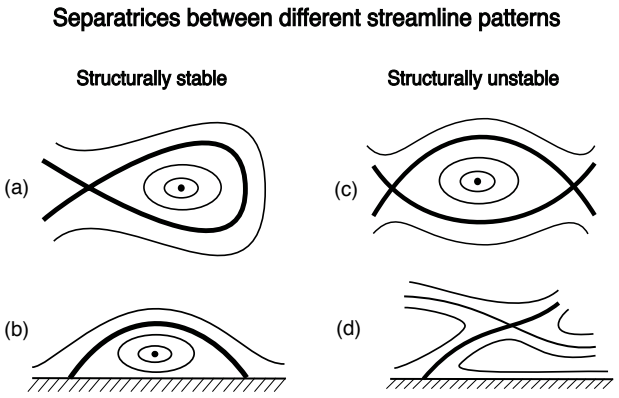

Figure 2.3 Structurally stable and unstable separatrices between instantaneous streamline patterns of 2D incompressible flows. (a) Streamline homoclinic to a hyperbolic stagnation point; (b) Streamline connecting a free-slip or no-slip boundary to itself, acting as the boundary of a separation bubble; (c) Heteroclinic streamlines between two hyperbolic stagnation points; (d) Heteroclinic streamline between a free-slip or no-slip boundary and a hyperbolic stagnation point.

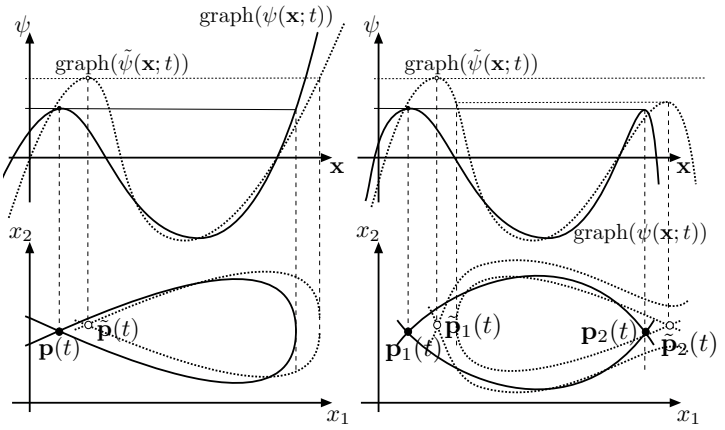

Figure 2.4 (Left) Under a small perturbation $\tilde{\psi}(\mathbf{x},t)$ of a stream function $\psi(\mathbf{x},t)$, a homoclinic streamline emanating from a saddle-type stagnation point $\mathbf{p}(t)$ will persist as a nearby streamline homoclinic to a perturbed stagnation point $\tilde{\mathbf{p}}(t)$. (Right) Under a similar perturbation, a heteroclinic streamline connecting two saddle-type stagnation points, $\mathbf{p}_1(t)$ and $\mathbf{p}_2(t)$, will generically break into a homoclinic streamline connecting $\tilde{\mathbf{p}}_2(t)$ to itself and a pair of locally open streamlines emanating from $\tilde{\mathbf{p}}_1(t)$.

2.1.3 Streamsurfaces and Stagnation Points in 3D Flows

A 2D surface that is everywhere tangential to the velocity field $\mathbf{v}(\mathbf{x},t)$ at time t is called an instantaneous *streamsurface*. All streamsurfaces are composed entirely of streamlines, including possible stagnation points. For this reason, streamsurfaces are invariant sets of the ODE (2.3).

https://doi.org/10.1017/9781009225199.003 Published online by Cambridge University Press

Stagnation points continue to be the most important building blocks of the global streamline and streamsurface geometry in 3D flows. As in 2D flows, instantaneous stagnation points are defined by the equation

$$\mathbf{v}(\mathbf{p}(t),t) = \mathbf{0}. \tag{2.11}$$

The local geometry of streamlines near stagnation points can again be identified from the linear stability analysis of the linearized streamline equation

$$\boldsymbol{\xi}' = \boldsymbol{\nabla}\mathbf{v}(\mathbf{p}(t),t)\boldsymbol{\xi}, \qquad \boldsymbol{\xi} \in \mathbb{R}^3 \tag{2.12}$$

at the stagnation point $\mathbf{p}(t)$.

At any point in the flow, the eigenvalues of the velocity gradient $\boldsymbol{\nabla}\mathbf{v}$ satisfy the characteristic equation

$$\lambda^3 - (\boldsymbol{\nabla}\cdot\mathbf{v})\,\lambda^2 + \frac{1}{2}\Big[\,(\boldsymbol{\nabla}\cdot\mathbf{v})^2 + |\mathbf{W}|^2 - |\mathbf{S}|^2\Big]\lambda - \det\boldsymbol{\nabla}\mathbf{v} = 0, \tag{2.13}$$

with the tensors $\mathbf{W}$ and $\mathbf{S}$ defined in Eq. (2.1) (see, e.g., Chong et al., 1990). For incompressible flows, we have $\boldsymbol{\nabla}\cdot\mathbf{v} = 0$ and hence the characteristic equation (2.13) simplifies to

$$\lambda^3 + \frac{1}{2}\Big[\,|\mathbf{W}|^2 - |\mathbf{S}|^2\Big]\lambda - \det\boldsymbol{\nabla}\mathbf{v} = 0. \tag{2.14}$$

Based on the eigenvalue configuration of $\boldsymbol{\nabla}\mathbf{v}(\mathbf{p}(t),t)$ determined by Eq. (2.14), Fig. 2.5 shows the four possible instantaneous streamline patterns near a hyperbolic stagnation point of an incompressible flow. Just as in 2D flows, a hyperbolic stagnation point is a solution $\mathbf{p}(t)$ of (2.11) at which the velocity gradient $\boldsymbol{\nabla}\mathbf{v}(\mathbf{p}(t),t)$ has no eigenvalues on the imaginary axis of the complex plane.

Perry and Chong (1987) give a more complete classification of local streamline geometries, including some non-hyperbolic (and hence structurally unstable; see §2.2.7) stagnation points as well. Surana et al. (2006) show that, after an appropriate rescaling near a no-slip boundary, the streamline patterns in Fig. 2.5 also arise near generic instantaneous separation and attachment points on free-slip boundaries.

Importantly, the linear stability analysis leading to the local streamline patterns in Fig. 2.5 is only relevant for fluid particle motion near stagnation points of steady flows, as we discuss later in §2.2.8. The Perry–Chong classification has nevertheless been broadly invoked in the literature for unsteady flows and for domains away from stagnation point. Both of these practices are unjustified and generally lead to incorrect results.

2.1.4 Irrotational and Inviscid Flows

We call a velocity field $\mathbf{v}$ *irrotational* if it is curl-free, i.e., $\boldsymbol{\omega}(\mathbf{x},t) = \boldsymbol{\nabla}\times\mathbf{v}(\mathbf{x},t) \equiv 0$. For 3D irrotational flows defined on a simply connected domain D,[1] there exists a *velocity potential* $\phi(\mathbf{x},t)$ such that the velocity field can be written as

$$\mathbf{v}(\mathbf{x},t) = \boldsymbol{\nabla}\phi(\mathbf{x},t). \tag{2.15}$$

[1] The domain D may either be the whole space or must have boundary components to which $\mathbf{v}$ is everywhere tangent (Stevenson, 1954; Tran-Cong, 1990; Mackay, 1994).

https://doi.org/10.1017/9781009225199.003 Published online by Cambridge University Press

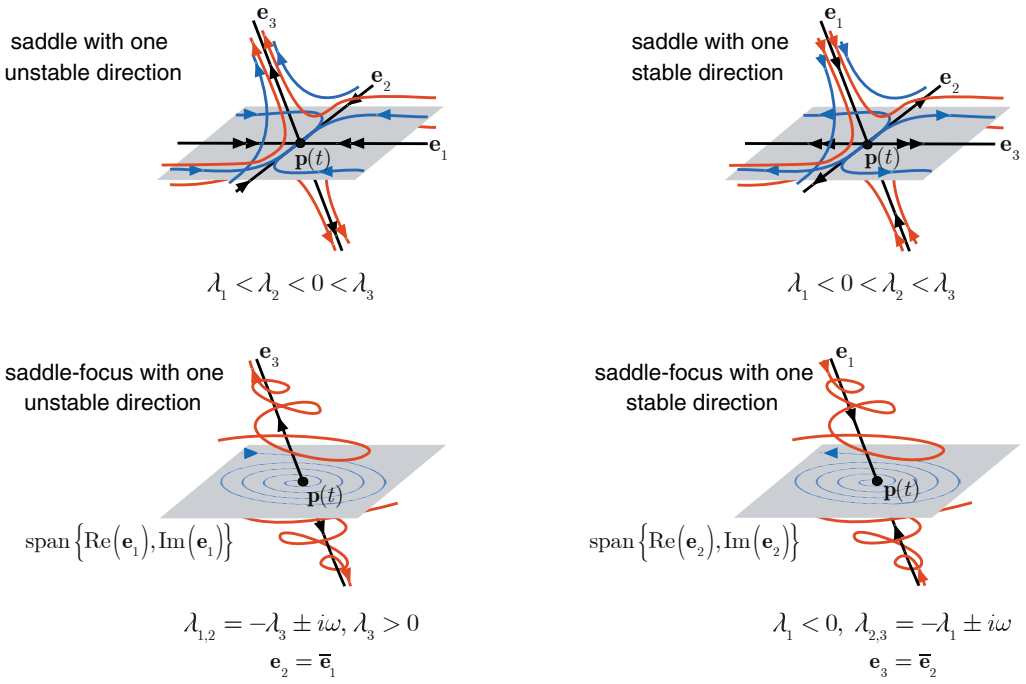

Figure 2.5 The four possible instantaneous streamline patterns near a hyperbolic stagnation point $\mathbf{p}(t)$ of a 3D incompressible flow. The eigenvalues and unit eigenvectors of $\nabla\mathbf{v}(\mathbf{p}(t),t)$ are denoted by λ_j and $\mathbf{e}_j$, respectively.

On any bounded domain D, a smooth velocity field $\mathbf{v}$ can always be decomposed into the sum of an incompressible and an irrotational component. Specifically, by the Helmholtz–Hodge decomposition theorem (see Chorin and Marsden, 1993), there exists a velocity field $\mathbf{w}(\mathbf{x},t)$ and a smooth scalar field $\sigma(\mathbf{x},t)$ such that

$$\mathbf{v} = \mathbf{w} + \nabla\sigma, \qquad \nabla \cdot \mathbf{w} \equiv 0,$$

and $\mathbf{w}$ is tangent to the boundary ∂D of the domain. We call an incompressible velocity field $\mathbf{v}$ *inviscid* if it satisfies the incompressible Navier–Stokes equation with zero viscosity ($\nu = 0$), i.e., it solves the *Euler equation*,

$$\partial_t \mathbf{v} + (\nabla\mathbf{v})\,\mathbf{v} = -\frac{1}{\rho}\nabla p + \mathbf{g}, \tag{2.16}$$

for an appropriate pressure field p, density field ρ and external body force-density field $\rho\mathbf{g}$.

2.2 Lagrangian Description of Fluid Motion

Fluid elements advected by the velocity field $\mathbf{v}(\mathbf{x},t)$ move along *fluid trajectories*. Therefore, trajectories are time-parametrized curves $\{\mathbf{x}(t)\}_{t\in\mathbb{R}}$ that solve the differential equation

$$\dot{\mathbf{x}} = \mathbf{v}(\mathbf{x},t), \tag{2.17}$$

https://doi.org/10.1017/9781009225199.003 Published online by Cambridge University Press

with the dot referring to differentiation with respect to the time t. If $\mathbf{v}(\mathbf{x}, t)$ is smooth,[2] then the ODE (2.17) has a unique trajectory $\mathbf{x}(t; t_0, \mathbf{x}_0)$ for any initial trajectory position $\mathbf{x}_0 \in U$ and initial time $t_0 \in [t_1, t_2]$, as shown in Fig. 2.1. As a consequence, no trajectory of the ODE (2.17) can cross another trajectory. Such an intersection would violate the uniqueness of solutions of Eq. (2.17). Physically, this nonuniqueness would imply that two initially different fluid elements end up occupying the same location $\mathbf{x}$ at the same time t.

The requirement of uniqueness for fluid element motion, however, does not prevent the same trajectory or other trajectories to traverse through the same location $\mathbf{x}$ at different times, as we indicated in the left subplot of Fig. 2.1. As a consequence, plots of trajectories of the ODE (2.17) (called *pathlines* in this context) can contain a number of self intersections, as well as mutual intersections.

2.2.1 Steady Flows as Autonomous Dynamical Systems

For steady velocity fields $\mathbf{v}(\mathbf{x})$, Eq. (2.17) becomes an *autonomous dynamical system* of the form

$$\dot{\mathbf{x}} = \mathbf{v}(\mathbf{x}), \tag{2.18}$$

with no explicit dependence on time. Trajectory evolution in Eq. (2.18) only depends on the elapsed time $t - t_0$, with no explicit dependence on the initial time t_0. Without loss of generality, therefore, the $t_0 = 0$ initial time can be selected for all trajectories, whose general form, $\mathbf{x}(t; \mathbf{x}_0)$, now depends only on the present time and the initial condition. This also implies that pathlines of ODE (2.18) cannot intersect each other or themselves by uniqueness of solutions.[3]

On a related note, separatrices in 2D flows (see Fig. 2.3 and the related discussion) are sometimes characterized as barriers to advective transport, i.e., they cannot be crossed by other trajectories of Eq. (2.18). This characterization of separatrices, however, is self-evident: no trajectory of Eq. (2.18) can be crossed by other trajectories by the uniqueness of solutions, as we have already mentioned. Instead, separatrices are distinguished because they act as boundaries between regions with different trajectory-topologies.

For a steady velocity field, $\mathbf{v}(\mathbf{x})$, fluid trajectories coincide with streamlines because the differential equations (2.3) and (2.17) coincide for such velocity fields. For 2D steady flows, formula (2.5) then implies the conservation of the stream function $\psi(\mathbf{x})$, forcing trajectories of $\mathbf{v}(\mathbf{x})$ to remain in level curves of $\psi(\mathbf{x})$ for all times. For unsteady flows, however, the two differential equations (2.3) and (2.17) no longer coincide and hence fluid trajectories will differ from streamlines. Trajectories can only be expected to stay close to streamlines temporarily in flow regions in which $\mathbf{v}(\mathbf{x}, t)$ is slowly varying in time.

[2] It is enough if $\mathbf{v}(\mathbf{x}, t)$ is *locally Lipschitz* in $\mathbf{x}$ near $\mathbf{x}_0$ and continuous in t at t_0 (see Arnold, 1978). The local Lipschitz condition at a point $\mathbf{x}_0$ requires the existence, for some finite time interval $[t_0 - \Delta, t_0 + \Delta]$, of a small open neighborhood $U_{\mathbf{x}_0}$ around $\mathbf{x}$ and a constant $L_{\mathbf{x}_0} > 0$ such that for any two points $\mathbf{x}_1, \mathbf{x}_2 \in U_{\mathbf{x}}$ and for all times $t \in [t_0 - \Delta, t_0 + \Delta]$, we have $|\mathbf{v}(\mathbf{x}_2, t) - \mathbf{v}(\mathbf{x}_1, t)| \leq L_{\mathbf{x}_0} |\mathbf{x}_2 - \mathbf{x}_1|$.

[3] At such an intersection, the same initial time $t_0 = 0$ could be selected for both trajectories, and hence the two trajectories through the intersection point would represent two different solutions to the same initial value problem.

https://doi.org/10.1017/9781009225199.003 Published online by Cambridge University Press

2.2.2 The Extended Phase Space

Any unsteady velocity field $\mathbf{v}(\mathbf{x}, t)$ can also be viewed as a steady velocity field on the *extended phase space* of the $(\mathbf{x}, t)$ variables. Indeed, letting

$$\mathbf{X} = \begin{pmatrix} \mathbf{x} \\ t \end{pmatrix}, \qquad \mathbf{V}(\mathbf{X}) = \begin{pmatrix} \mathbf{v}(\mathbf{x}, t) \\ 1 \end{pmatrix}, \tag{2.19}$$

we obtain the autonomous dynamical system

$$\dot{\mathbf{X}} = \mathbf{V}(\mathbf{X}), \tag{2.20}$$

with $\mathbf{X} \in U \times \mathbb{R}$, where $U \subset \mathbb{R}^n$ is the domain of definition of the unsteady vector field. Note that $\boldsymbol{\nabla}_{\mathbf{X}} \cdot \mathbf{V} = \boldsymbol{\nabla} \cdot \mathbf{v}$. Thus the divergence of the velocity field is preserved under this extension.

The conversion of an unsteady flow into a steady flow on a higher-dimensional system has several advantages but does not provide a universal vehicle for extending the properties of steady flows defined on U to unsteady flows. One of the reasons for this is that the steady extended system (2.20) has a higher dimension and hence its trajectories can display a higher level of topological and dynamical complexity than steady flows defined on U.

Another reason is that a number of useful properties of steady flows (e.g., recurrence and ergodicity) that we will see later are only valid or defined on compact domains that are invariant under the trajectories of the velocity field. No such compact invariant domain will exist for the extended system (2.20) because all its trajectories become unbounded in the t direction. This unboundedness issue can only be remedied for time-periodic and time-quasiperiodic velocity fields, for which the time-dependence of $\mathbf{v}(\mathbf{x}, t)$ can be confined to a compact set (the circle or the torus), as we will see in §2.2.12.

2.2.3 The Flow Map and Its Gradient

The evolution of a trajectory $\mathbf{x}(t; t_0, \mathbf{x}_0)$ as a function of its initial position is described by the *flow map*

$$\mathbf{F}_{t_0}^{t} : \mathbf{x}_0 \mapsto \mathbf{x}(t; t_0, \mathbf{x}_0), \tag{2.21}$$

which is well defined for any time t, as long as the trajectory stays in a compact domain U where the underlying velocity field $\mathbf{v}(\mathbf{x}, t)$ is known.[4] By the definition of $\mathbf{F}_{t_0}^{t}$, we have the relation

$$\frac{d}{dt}\mathbf{F}_{t_0}^{t}(\mathbf{x}_0) = \mathbf{v}\left(\mathbf{F}_{t_0}^{t}(\mathbf{x}_0), t\right). \tag{2.22}$$

By fundamental results for differential equations, the flow map $\mathbf{F}_{t_0}^{t}$ is as smooth with respect to initial conditions and velocity field parameters as $\mathbf{v}(\mathbf{x}, t)$ is with respect to $\mathbf{x}$ and the same flow parameters, respectively (see Arnold, 1978).

We call the domain U *invariant* under the flow if the velocity field $\mathbf{v}$ along ∂U is tangent to ∂U for all times. This implies that for all times in $[t_1, t_2]$, trajectories starting in U remain

[4] $\mathbf{F}_{t_0}^{t}(\mathbf{x}_0)$ may generally become undefined for increasing t due to a finite-time blow-up of trajectories, even if the velocity field is smooth (consider, e.g., the simple scalar ODE $\dot{x} = 1 + x^2$). However, no finite-time blow-up is possible as long as the trajectory is confined to a compact flow domain U (see, e.g., Arnold, 1978).

https://doi.org/10.1017/9781009225199.003 Published online by Cambridge University Press

in U and trajectories starting in ∂U remain in ∂U. For autonomous dynamical systems of the form (2.18), the flow map can simply be defined as

$$\mathbf{F}^t : \mathbf{x}_0 \mapsto \mathbf{x}(t; 0, \mathbf{x}_0), \tag{2.23}$$

with the initial time always taken to be $t_0 = 0$. In this case, the flow map becomes a one-parameter family of transformations, as opposed to a two-parameter family of transformations in the nonautonomous case.

As long as it is well defined, the flow map is a *diffeomorphism*: it is as smooth as the velocity field and has an equally smooth inverse $\left(\mathbf{F}_{t_0}^t\right)^{-1} = \mathbf{F}_t^{t_0}$, the mapping taking current positions at time t back to their initial positions at time t_0. Flow maps between two arbitrary times are orientation preserving and can be concatenated to give one net flow map for the displacement of a fluid element. These two properties can be formally stated as

$$\det \nabla \mathbf{F}_s^t > 0, \quad \mathbf{F}_s^t \left(\mathbf{F}_{t_0}^s(\mathbf{x}_0)\right) = \mathbf{F}_{t_0}^t(\mathbf{x}_0), \tag{2.24}$$

for any choice of the times $t_0, s, t \in [t_1, t_2]$; see, e.g., Arnold (1978) for proofs of these statements.

The flow map $\mathbf{F}_{t_0}^t$ does not inherit the time-dependence of the velocity field $\mathbf{v}(\mathbf{x}, t)$. Indeed, a steady velocity field $\mathbf{v}(\mathbf{x})$ with no explicit time dependence already generates a flow map $\mathbf{F}^t$ with general (aperiodic) time dependence. Similarly, time-periodic and time-quasiperiodic velocity fields generate flow maps with general time dependence. Nevertheless, the flow map $\mathbf{F}^t$ of a steady velocity field will become a steady map (the identity map) when evaluated on specific initial conditions (fixed points) of the flow (see §2.2.11). Similarly, the time-dependent image, $\mathbf{F}_{t_0}^t(\mathbf{x}_0)$, of an initial condition in a time-periodic velocity field is time-periodic for exceptional $\mathbf{x}_0$ initial conditions that lie on periodic orbits of $\mathbf{v}(\mathbf{x}, t)$ (see §2.2.12).

The derivative $\nabla \mathbf{F}_{t_0}^t(\mathbf{x}_0)$ of the flow map with respect to its argument $\mathbf{x}_0$ is the *deformation gradient*. Technically, $\nabla \mathbf{F}_{t_0}^t(\mathbf{x}_0)$ is a *two-point tensor* (see §3.5 for more detail) that maps vectors in the tangent space $T_{\mathbf{x}_0}\mathbb{R}^n$ of $\mathbb{R}^n$ at $\mathbf{x}_0$ to vectors in the tangent space $T_{\mathbf{F}_{t_0}^t(\mathbf{x}_0)}\mathbb{R}^n$ of $\mathbb{R}^n$ at the advected position $\mathbf{F}_{t_0}^t(\mathbf{x}_0)$.[5] More formally, therefore, $\nabla \mathbf{F}_{t_0}^t$ is defined as

$$\begin{aligned} \nabla \mathbf{F}_{t_0}^t : T_{\mathbf{x}_0}\mathbb{R}^n &\to T_{\mathbf{F}_{t_0}^t(\mathbf{x}_0)}\mathbb{R}^n, \\ \boldsymbol{\xi}_0 &\mapsto \nabla \mathbf{F}_{t_0}^t(\mathbf{x}_0)\boldsymbol{\xi}_0, \end{aligned} \tag{2.25}$$

mapping vectors $\boldsymbol{\xi}_0$ based at $\mathbf{x}_0$ to vectors based at $\mathbf{F}_{t_0}^t(\mathbf{x}_0)$, as shown in Fig. 2.6. Physically, an initial infinitesimal perturbation, $\boldsymbol{\xi}_0$, to the initial condition $\mathbf{x}_0$ at time t_0 evolves into a perturbation $\nabla \mathbf{F}_{t_0}^t(\mathbf{x}_0)\boldsymbol{\xi}_0$ to the trajectory location $\mathbf{x}(t; t_0, \mathbf{x}_0)$ at time t.

The deformation gradient also allows us to express the derivative of the flow map $\mathbf{F}_{t_0}^t$ with respect to the initial time t_0. Indeed, differentiating the identity $\mathbf{F}_{t_0}^t \left(\mathbf{F}_t^{t_0}(\mathbf{x})\right) = \mathbf{x}$ with respect to t_0 gives the relationship

$$\frac{d}{dt_0}\mathbf{F}_{t_0}^t(\mathbf{x}_0) = -\nabla \mathbf{F}_{t_0}^t(\mathbf{x}_0)\mathbf{v}(\mathbf{x}_0, t_0). \tag{2.26}$$

For a steady velocity field $\mathbf{v}(\mathbf{x})$, this relationship simplifies to

$$\frac{d}{dt_0}\mathbf{F}_{t_0}^t(\mathbf{x}_0) = -\mathbf{v}(\mathbf{F}_{t_0}^t(\mathbf{x}_0)),$$

[5] See Appendix A.4 for a brief summary of concepts from differential geometry, including tangent spaces of $\mathbb{R}^n$, that are relevant for derivatives of mappings between manifolds.

https://doi.org/10.1017/9781009225199.003 Published online by Cambridge University Press

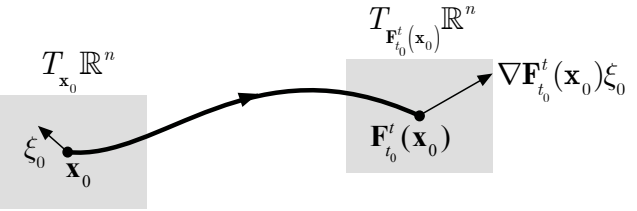

Figure 2.6 The definition of the deformation gradient.

given that $\mathbf{v}(\mathbf{F}_{t_0}^t(\mathbf{x}_0)) = \boldsymbol{\nabla}\mathbf{F}_{t_0}^t(\mathbf{x}_0)\mathbf{v}(\mathbf{x}_0, t_0)$ holds, as we will deduce later in formula (2.55).

As a mapping between two different linear spaces, $\boldsymbol{\nabla}\mathbf{F}_{t_0}^t(\mathbf{x}_0)$ does not have well-defined eigenvalues and eigenvectors, even though they are sometimes erroneously introduced in the literature for its specific matrix representations. Indeed, it is tempting to introduce coordinates in the domain space $T_{\mathbf{x}_0}\mathbb{R}^n$ and the range space $T_{\mathbf{F}_{t_0}^t(\mathbf{x}_0)}\mathbb{R}^n$, then solve a formal eigenvalue problem for the linear map $\boldsymbol{\nabla}\mathbf{F}_{t_0}^t(\mathbf{x}_0)$ in those coordinates. These formally computed eigenvalues and eigenvectors, however, will depend on the coordinates introduced and hence will no longer be invariants of $\boldsymbol{\nabla}\mathbf{F}_{t_0}^t(\mathbf{x}_0)$. The eigenvalues and eigenvectors of $\boldsymbol{\nabla}\mathbf{F}_{t_0}^t(\mathbf{x}_0)$ are only well defined in a coordinate-free fashion if $T_{\mathbf{x}_0}\mathbb{R}^n \equiv T_{\mathbf{F}_{t_0}^t(\mathbf{x}_0)}\mathbb{R}^n$ holds, i.e., the trajectory $\mathbf{x}(t; t_0, \mathbf{x}_0)$ returns to its initial position $\mathbf{x}_0$ at time t. Even then, the eigenvalues are irrelevant for the long-term evolution for the perturbation $\boldsymbol{\xi}_0$ to $\mathbf{x}_0$ unless the velocity field $\mathbf{v}(\mathbf{x}, t)$ is time-periodic with period $T = t - t_0$, and hence $\mathbf{x}(t; t_0, \mathbf{x}_0)$ is a periodic trajectory. In that case, $\mathbf{F}_{t_0}^t(\mathbf{x}_0)$ is a period-t map or Poincaré map, as discussed in §2.2.12.

In contrast, the velocity gradient $\boldsymbol{\nabla}\mathbf{v}(\mathbf{x}, t)$ discussed in §3.3 is a linear operator mapping the tangent space $T_{\mathbf{x}}\mathbb{R}^n$ into itself and hence $\boldsymbol{\nabla}\mathbf{v}(\mathbf{x}, t)$ admits well-defined eigenvalues and eigenvectors.

2.2.4 Material Surfaces, Material Lines and Streaklines

A *material surface* $\mathcal{M}(t)$ is an evolving surface of fluid particles that move from their initial positions along trajectories of the velocity field $\mathbf{v}$. More precisely,

$$\mathcal{M}(t) = \mathbf{F}_{t_0}^t(\mathcal{M}_0), \quad \mathcal{M}_0 = \mathcal{M}(t_0). \tag{2.27}$$

As shown in Fig. 2.7, the surface $\mathcal{M}(t)$ is a smooth manifold if $\mathcal{M}_0$ is a smooth manifold, because the flow map $\mathbf{F}_{t_0}^t$ is a diffeomorphism. In that case, $\mathbf{F}_{t_0}^t$ is a smooth mapping between manifolds and hence $\boldsymbol{\nabla}\mathbf{F}_{t_0}^t(\mathbf{x}_0)$ maps the *tangent space* $T_{\mathbf{x}_0}\mathcal{M}_0$ of $\mathcal{M}_0$ at $\mathbf{x}_0$ onto the tangent space of $\mathcal{M}(t)$ at the point $\mathbf{F}_{t_0}^t(\mathbf{x}_0)$, i.e.,

$$\boldsymbol{\nabla}\mathbf{F}_{t_0}^t(\mathbf{x}_0)\, T_{\mathbf{x}_0}\mathcal{M}_0 = T_{\mathbf{F}_{t_0}^t(\mathbf{x}_0)}\mathcal{M}(t), \tag{2.28}$$

as shown in Fig. 2.7 (see Abraham et al., 1988).

Let $N_{\mathbf{x}_0}\mathcal{M}_0$ denote the *normal space* of $\mathcal{M}_0$ at $\mathbf{x}_0$, defined as the orthogonal complement of $T_{\mathbf{x}_0}\mathcal{M}_0$ in the ambient space $\mathbb{R}^n$, as shown in Fig. 2.7 (see also Appendix A.4). Consequently, if $\mathbf{a}$ is a vector in $T_{\mathbf{x}_0}\mathcal{M}_0$ and $\mathbf{b}$ is a vector in $N_{\mathbf{x}_0}\mathcal{M}_0$, then the inner product of these vectors must vanish by their orthogonality: $\langle \mathbf{a}, \mathbf{b} \rangle = 0$. This identity can be written equivalently as

https://doi.org/10.1017/9781009225199.003 Published online by Cambridge University Press

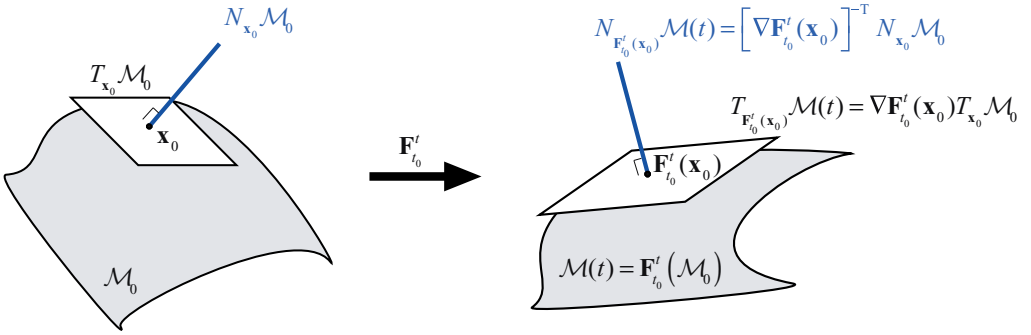

Figure 2.7 Geometry near a material surface $\mathcal{M}(t)$. Tangent and normal spaces at the same material point of this evolving surface are mapped into each other by the deformation gradient $\nabla\mathbf{F}^t_{t_0}$ and by its inverse transpose, $\left[\nabla\mathbf{F}^t_{t_0}\right]^{-\mathrm{T}}$, respectively.

$$\langle \mathbf{b}, \mathbf{a}\rangle = \left\langle \mathbf{b}, \left[\nabla\mathbf{F}^t_{t_0}(\mathbf{x}_0)\right]^{-1} \nabla\mathbf{F}^t_{t_0}(\mathbf{x}_0)\mathbf{a}\right\rangle = \left\langle \left[\nabla\mathbf{F}^t_{t_0}(\mathbf{x}_0)\right]^{-\mathrm{T}} \mathbf{b}, \nabla\mathbf{F}^t_{t_0}(\mathbf{x}_0)\mathbf{a}\right\rangle = 0, \tag{2.29}$$

where $-\mathrm{T}$ denotes inverse transpose. Note that $\mathbf{a} \in T_{\mathbf{x}_0}\mathcal{M}_0$ and $\mathbf{b} \in N_{\mathbf{x}_0}\mathcal{M}_0$ are arbitrary in the relationship (2.29), and hence Eq. (2.28) implies that $\left[\nabla\mathbf{F}^t_{t_0}(\mathbf{x}_0)\right]^{-\mathrm{T}} \mathbf{b} \in N_{\mathbf{F}^t_{t_0}(\mathbf{x}_0)}\mathcal{M}(t)$.

Therefore, we have obtained that any vector $\mathbf{b} \in N_{\mathbf{x}_0}\mathcal{M}_0$ is mapped by $\left[\nabla\mathbf{F}^t_{t_0}(\mathbf{x}_0)\right]^{-\mathrm{T}}$ into a vector normal to $T_{\mathbf{F}^t_{t_0}(\mathbf{x}_0)}\mathcal{M}(t)$, or, equivalently,

$$\left[\nabla\mathbf{F}^t_{t_0}(\mathbf{x}_0)\right]^{-\mathrm{T}} N_{\mathbf{x}_0}\mathcal{M}_0 = N_{\mathbf{F}^t_{t_0}(\mathbf{x}_0)}\mathcal{M}(t)\,. \tag{2.30}$$

In other words, a normal of a material surface at the point $\mathbf{x}_0$ at time t_0 is advected by the inverse transpose $\left[\nabla\mathbf{F}^t_{t_0}(\mathbf{x}_0)\right]^{-\mathrm{T}}$ of the deformation gradient to a normal to the same material surface at the point $\mathbf{F}^t_{t_0}(\mathbf{x}_0)$ at time t. Consequently, as illustrated in Fig. 2.7, we also have

$$\left[\nabla\mathbf{F}^t_{t_0}(\mathbf{x}_0)\right]^{\mathrm{T}} N_{\mathbf{F}^t_{t_0}(\mathbf{x}_0)}\mathcal{M}(t) = N_{\mathbf{x}_0}\mathcal{M}_0. \tag{2.31}$$

Since $\mathcal{M}_0$ was arbitrary in this argument, so was the subspace $N_{\mathbf{x}_0}\mathcal{M}_0 \subset T_{\mathbf{x}_0}\mathbb{R}^n$. Therefore, the linear mapping $\left[\nabla\mathbf{F}^t_{t_0}(\mathbf{x}_0)\right]^{-\mathrm{T}}$ is defined for any vector $T_{\mathbf{x}_0}\mathbb{R}^n$ and maps any such vector into $T_{\mathbf{F}^t_{t_0}(\mathbf{x}_0)}\mathbb{R}^n$:

$$\left[\nabla\mathbf{F}^t_{t_0}(\mathbf{x}_0)\right]^{-\mathrm{T}} : T_{\mathbf{x}_0}\mathbb{R}^n \to T_{\mathbf{F}^t_{t_0}(\mathbf{x}_0)}\mathbb{R}^n. \tag{2.32}$$

Reversing the role of $\mathbf{x}_0$ and $\mathbf{F}^t_{t_0}(\mathbf{x}_0)$ in formula (2.32) leads to

$$\left[\nabla\mathbf{F}^t_{t_0}(\mathbf{x}_0)\right]^{\mathrm{T}} : T_{\mathbf{F}^t_{t_0}(\mathbf{x}_0)}\mathbb{R}^n \to T_{\mathbf{x}_0}\mathbb{R}^n, \tag{2.33}$$

showing that the transpose (or adjoint) of the deformation gradient can be viewed as a mapping of vectors in $T_{\mathbf{F}^t_{t_0}(\mathbf{x}_0)}\mathbb{R}^n$ back to $T_{\mathbf{x}_0}\mathbb{R}^n$.

https://doi.org/10.1017/9781009225199.003 Published online by Cambridge University Press

A more specific consequence of Eq. (2.30) is the following classic result: if $\mathbf{n}_0 \in N_{\mathbf{x}_0}\mathcal{M}_0$ is a unit normal to $\mathcal{M}_0$ to at $\mathbf{x}_0$, then the surface element $\mathbf{n}_0 dA_0$ of $\mathcal{M}_0$ at $\mathbf{x}_0$ is carried by the flow into the surface element

$$\mathbf{n}dA = \det \nabla \mathbf{F}_{t_0}^t(\mathbf{x}_0) \left[\nabla \mathbf{F}_{t_0}^t(\mathbf{x}_0)\right]^{-\mathrm{T}} \mathbf{n}_0 dA_0 \tag{2.34}$$

of $\mathcal{M}(t)$ at the point $\mathbf{F}_{t_0}^t(\mathbf{x}_0)$ (see Gurtin, 1981; Truesdell, 1992).

A *material line* (sometimes called a *timeline*) is an evolving curve composed of the same fluid particles, i.e., the image,

$$\mathcal{L}(t) = \mathbf{F}_{t_0}^t(\mathcal{L}(t_0)), \tag{2.35}$$

of a curve $\mathcal{L}(t_0)$ of initial particle particle positions under the flow map $\mathbf{F}_{t_0}^t$ (see Fig. 2.8).

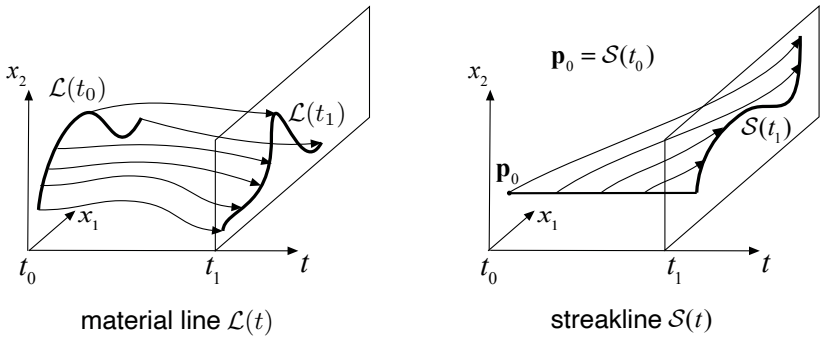

Figure 2.8 (Left) Material line $\mathcal{L}(t)$ evolving from its initial curve $\mathcal{L}(t_0)$, and (Right) a streakline $\mathcal{S}(t)$ evolving from its release location point $\mathbf{p}_0(t_0) = \mathcal{S}(t_0)$.

As we have seen for general material surfaces, $\nabla \mathbf{F}_{t_0}^t(\mathbf{x}_0)$ maps the tangent vector of $\mathcal{L}(t_0)$ at $\mathbf{x}_0$ into a tangent vector of $\mathcal{L}(t)$ at the point $\mathbf{F}_{t_0}^t(\mathbf{x}_0)$. Similarly, $\left[\nabla \mathbf{F}_{t_0}^t(\mathbf{x}_0)\right]^{-\mathrm{T}}$ maps a vector normal to $\mathcal{L}(t_0)$ at $\mathbf{x}_0$ to a vector normal to $\mathcal{L}(t)$ at the point $\mathbf{F}_{t_0}^t(\mathbf{x}_0)$ (see Fig. 2.7).

A *streakline* is a set formed of an increasing number of fluid particles, all released continually from the same point $\mathbf{p}_0$. Specifically, a streakline is a time-dependent curve $\mathcal{S}(t)$ defined as

$$\mathcal{S}(t) = \bigcup_{\tau \in [t_0, t]} \mathbf{F}_\tau^t(\mathbf{p}_0), \tag{2.36}$$

as illustrated in Fig. 2.8. As a consequence of this definition, for any fixed $\tau \in [t_0, t]$, the evolving subset $\mathcal{L}(t) = \mathbf{F}_\tau^t(\mathcal{S}(\tau))$ of a streakline $\mathcal{S}(t)$ is a material line. Yet $\mathcal{S}(t)$ itself is not a material line, given that it contains an increasing number of fluid particles over time.

We have already noted that full fluid trajectories (or pathlines), $\{\mathbf{x}(t)\}_{t \in \mathbb{R}}$, coincide with streamlines in steady flows. We further note here that in steady flows, a pathline emanating from a point $\mathbf{p}_0$ fills an increasing, one-sided subset of the streamline starting from $\mathbf{p}_0$ as the time increases. This is why streaklines are generally used to visualize pieces of streamlines in steady flows, as illustrated in Fig. 2.9.

While streamlines and streamsurfaces have the exact same type of time dependence as the underlying velocity field, no such conclusion can be drawn generally for general material lines, material surfaces and streaklines. This is because the flow map does not inherit the

https://doi.org/10.1017/9781009225199.003 Published online by Cambridge University Press

Figure 2.9 Streaklines used to visualize subsets of streamlines in a steady flow around a Nio ET7 electric vehicle. Image: Courtesy of Nio Inc.

time dependence of the underlying velocity field, as we have already noted in §2.2.3. Very special material lines and surfaces can, however, inherit the time-dependence of the velocity field. These will be precisely the advective transport barriers we will discuss in Chapter 4 for temporally recurrent flows.

2.2.5 Invariant Manifolds

An *invariant manifold* of a velocity field $\mathbf{v}(\mathbf{x}, t)$ is an evolving material set $\mathcal{M}(t) = \mathbf{F}_{t_0}^{t}(\mathcal{M}(t_0))$ that is a k-dimensional differentiable manifold (see Appendix A.4) at any fixed time $t \in [t_0, t_1]$. Therefore, a 1D invariant manifold is a material curve, a 2D invariant manifold is a material surface and a 3D invariant manifold is an evolving open subset of the flow domain in 3D fluid flows.

Because the flow map $\mathbf{F}_{t_0}^{t}$ is a diffeomorphism, any choice of a smooth set $\mathcal{M}(t_0)$ of initial conditions will generate an invariant manifold $\mathcal{M}(t)$ under $\mathbf{F}_{t_0}^{t}$ over any finite time interval $[t_0, t_1]$.[6] Therefore, there are infinitely many invariant manifolds through each point of a fluid flow. Of these, we are generally interested in the ones that have a strong impact on nearby trajectories and are robust under small perturbations to the flow. Over finite time intervals, there are different ways to define such a strong impact, which explains why this whole book is devoted to finding transport barriers as uniquely influential invariant manifolds. Our discussion will focus on techniques that render invariant manifolds that are robust, i.e., structurally stable; this notion is defined in §2.2.7.

2.2.6 Evolution of Material Volume and Mass

A subset V_0 of initial conditions will evolve under the flow map as a *material set*

$$V(t) = \mathbf{F}_{t_0}^{t}(V_0), \tag{2.37}$$

[6] This statement does not hold over infinite time intervals as the flow map is generally not even defined in that limit for most points.

https://doi.org/10.1017/9781009225199.003 Published online by Cambridge University Press

as shown in Fig. 2.10. The rate of change of the material volume vol $(V(t))$ (or material area in 2D) can be computed as

$$\begin{aligned}\frac{d}{dt}\text{vol}\,(V(t)) &= \frac{d}{dt}\int_{V(t)} dV = \frac{d}{dt}\int_{V_0} \det \nabla \mathbf{F}_{t_0}^t(\mathbf{x}_0)\; dV_0 = \int_{V_0} \frac{d}{dt}\det \nabla \mathbf{F}_{t_0}^t(\mathbf{x}_0)\; dV_0 \\ &= \int_{V(t)} \frac{\frac{d}{dt}\det \nabla \mathbf{F}_{t_0}^t(\mathbf{x}_0)}{\det \nabla \mathbf{F}_{t_0}^t(\mathbf{x}_0)}\, dV \\ &= \int_{V(t)} \boldsymbol{\nabla}\cdot \mathbf{v}(\mathbf{x},t)\, dV,\end{aligned} \tag{2.38}$$

where we have used the classic formula $dV = \det \nabla \mathbf{F}_{t_0}^t(\mathbf{x}_0)\; dV_0$ for the change of variables defined by $\mathbf{x} = \mathbf{F}_{t_0}^t(\mathbf{x}_0)$, and formula (2.50) to compute $\frac{d}{dt}\det \nabla \mathbf{F}_{t_0}^t$. The volume evolution formula (2.38) is often referred to as *Liouville's theorem* in the dynamical systems literature (see, e.g., Arnold, 1978).

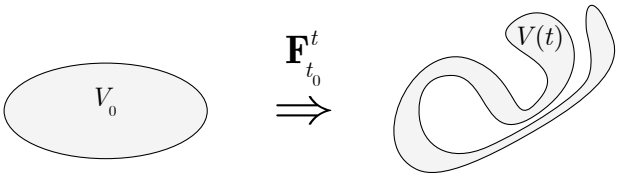

Figure 2.10 Material set $V(t)$ evolving under the flow map $\mathbf{F}_{t_0}^t$.

We will mostly assume that the flow is *incompressible*, i.e., the velocity field is divergence free:

$$\nabla \cdot \mathbf{v} = 0. \tag{2.39}$$

Under this incompressibility assumption, the formulas (2.50) and (2.38) imply the local and global forms of the conservation of material volume:

$$\det \nabla \mathbf{F}_{t_0}^t(\mathbf{x}_0) \equiv 1, \quad \text{vol}\, V(t) \equiv \text{vol}\, V_0 \tag{2.40}$$

for all points $\mathbf{x}_0$ and all subsets V_0 of U. For 2D flows, the volume is to be replaced with area in these statements.

In most applications, even compressible flows are *mass preserving*, with their mass-density field $\rho(\mathbf{x},t)$ satisfying the *equation of continuity*

$$\partial_t \rho + \boldsymbol{\nabla}\cdot(\rho \mathbf{v}) = 0. \tag{2.41}$$

The equation of continuity (2.41) together with (2.50) then yields a relation between the evolution of the density along trajectories and the deformation gradient:

$$\rho\left(\mathbf{F}_{t_0}^t(\mathbf{x}_0),t\right) = \rho_0(\mathbf{x}_0)\exp\left[-\int_{t_0}^t \boldsymbol{\nabla}\cdot\mathbf{v}\left(\mathbf{F}_{t_0}^s(\mathbf{x}_0),s\right)\, ds\right] = \frac{\rho_0(\mathbf{x}_0)}{\det \boldsymbol{\nabla}_0 \mathbf{F}_{t_0}^t(\mathbf{x}_0)}. \tag{2.42}$$

An evolving material volume $V(t)$ of a mass-conserving flow then obeys the conservation law

$$\int_{V(t)} \rho(\mathbf{x},t)\, dV = \int_{V_0} \rho_0(\mathbf{x}_0)\, dV_0, \tag{2.43}$$

https://doi.org/10.1017/9781009225199.003 Published online by Cambridge University Press

obtained by changing the variables of integration from $\mathbf{x}$ to $\mathbf{x}_0$ and using formula (2.42).

2.2.7 Topological Equivalence and Structural Stability

Topological equivalence seeks to formalize the notion of similar behavior in different flows. The idea is to consider one flow to be equivalent to another flow if their trajectory structures are the same up to a continuous deformation that keeps the orientation of the trajectories.

Specifically, two steady velocity fields, $\mathbf{v}(\mathbf{x})$ and $\mathbf{w}(\mathbf{x})$, defined on a compact domain $U \subset \mathbb{R}^n$ are said to be *topologically equivalent* over a time interval $[t_0, t_1]$ if there exists a homeomorphism (i.e., a continuous map with a continuous inverse) $\mathbf{h}\colon U \to U$ that transforms the oriented trajectories of $\mathbf{v}(\mathbf{x})$ into the oriented trajectories of $\mathbf{w}(\mathbf{x})$. In particular, if $\mathbf{F}^t$ is the flow map of $\mathbf{v}$ and $\mathbf{G}^t$ is the flow map of $\mathbf{w}$, then topological equivalence between the two flows requires the existence of a function $\mathbf{h}$ as above, along with a monotonically increasing, scalar-valued function $\tau(\mathbf{x}, t)$ on $U \times [t_0, t_1]$, such that

$$\mathbf{h}\left(\mathbf{F}^{\tau(\mathbf{x}_0,t)}(\mathbf{x}_0)\right) = \mathbf{G}^t(\mathbf{h}(\mathbf{x}_0)) \tag{2.44}$$

for all $\mathbf{x}_0 \in U$ and all $t \in [t_0, t_1]$. The notion of topological equivalence of unsteady velocity fields is more involved and will not be discussed here.[7]

Topological equivalence can be used to express the robustness of a flow on its compact domain of definition U. Namely, the velocity field $\mathbf{v}(\mathbf{x})$ is called *a structurally stable velocity field* if any other velocity field on U that is close enough to $\mathbf{v}$ in the C^1 norm is also topologically equivalent to $\mathbf{v}$. For instance, any steady velocity field is structurally stable in some vicinity of its saddle-type stagnation points. Also, any planar incompressible velocity field is structurally stable (within the family of incompressible, steady velocity fields) in a vicinity of its center-type stagnation points.

We will also use the notion of structural stability for individual invariant sets of $\mathbf{v}(\mathbf{x}, t)$. We call a material set $X(t) \subset \mathbb{R}^n$ (see formula (2.37) for a definition) over a finite time interval $t \in [t_0, t_1]$ a *structurally stable set* if it smoothly persists under small enough perturbations of $\mathbf{v}(\mathbf{x}, t)$. Specifically, X is structurally stable if for any velocity field $\mathbf{w}(\mathbf{x}, t)$ close enough in the C^1 norm to $\mathbf{v}(\mathbf{x}, t)$, there exists a nearby material set $Y(t)$ for the flow map $\mathbf{G}^t_{t_0}$ (i.e., $\mathbf{G}^t_{t_0}(Y(t_0)) = Y(t)$ for all $t \in [t_0, t_1]$) such that $Y(t)$ is C^r diffeomorphic to $X(t)$ for all $t \in [t_0, t_1]$. Structurally stable invariant sets of steady velocity fields include saddle-type stagnation fields along with their local stable and unstable manifolds, homoclinic orbits, families of invariant tori within the class of volume-preserving velocity fields and limit cycles and attracting tori in compressible flows.

[7] For a nonautonomous velocity field $\mathbf{v}(\mathbf{x}, t)$ with flow map $\mathbf{F}^t_{t_0}$ and another velocity field $\mathbf{w}(\mathbf{x}, t)$ with flow map $\mathbf{G}^t_{t_0}$, it is tempting to define topological equivalence between $\mathbf{v}(\mathbf{x}, t)$ and $\mathbf{w}(\mathbf{x}, t)$ by requiring the time-dependent version of Eq. (2.44) to hold, i.e., $\mathbf{h}^{\tau(\mathbf{x}_0,t)}\left(\mathbf{F}^{\tau(\mathbf{x}_0,t)}_{t_0}(\mathbf{x}_0)\right) = \mathbf{G}^t_{t_0}(\mathbf{h}^t(\mathbf{x}_0))$ for all $\mathbf{x}_0 \in U$ and all $t \in [t_0, t_1]$. In that case, however, any $\mathbf{v}(\mathbf{x}, t)$ would be topologically equivalent to $\mathbf{w}(\mathbf{x}, t) \equiv \mathbf{0}$ via the homeomorphism family $\mathbf{h}^t = \mathbf{F}^{t_0}_t$ for any fixed t_0, as noted by Aulbach and Wanner (2000). Indeed, this choice of $\mathbf{h}^t$ would simply map any point $\mathbf{x}$ into the initial condition $\mathbf{x}_0$ at time t_0 of the trajectory that is at $\mathbf{x}$ at time t. Therefore, we would obtain $\frac{\partial}{\partial t} h^t(\mathbf{x}) \equiv \mathbf{0}$.

https://doi.org/10.1017/9781009225199.003 Published online by Cambridge University Press

2.2.8 Linearized Flow: The Equation of Variations

Infinitesimally small perturbations, $\boldsymbol{\xi}_0$, to an initial position $\mathbf{x}_0$ in the flow evolve in time as vectors $\boldsymbol{\xi}(t)$ along the trajectory $\mathbf{x}(t; t_0, \mathbf{x}_0)$. This evolution is described by the linearized version of the ODE (2.17), defined as the *equation of variations*

$$\dot{\boldsymbol{\xi}} = \boldsymbol{\nabla}\mathbf{v}(\mathbf{x}(t; t_0, \mathbf{x}_0), t)\boldsymbol{\xi}. \tag{2.45}$$

By direct substitution, one verifies that solutions of this linear ODE are of the form

$$\boldsymbol{\xi}(t) = \boldsymbol{\nabla}\mathbf{F}_{t_0}^{t}(\mathbf{x}_0)\,\boldsymbol{\xi}_0, \tag{2.46}$$

and hence the deformation gradient $\boldsymbol{\nabla}\mathbf{F}_{t_0}^{t}(\mathbf{x}_0)$ is the normalized fundamental matrix solution to the equation of variations. Differentiation of the second identity in Eq. (2.24) for the flow map implies a similar group property for the deformation gradient:

$$\boldsymbol{\nabla}\mathbf{F}_{t_0}^{t}(\mathbf{x}_0) = \boldsymbol{\nabla}\mathbf{F}_{s}^{t}\left(\mathbf{F}_{t_0}^{s}(\mathbf{x}_0)\right)\boldsymbol{\nabla}\mathbf{F}_{t_0}^{s}(\mathbf{x}_0). \tag{2.47}$$

We note that a direct substitution shows $\left[\boldsymbol{\nabla}\mathbf{F}_{t_0}^{t}(\mathbf{x}_0)\right]^{-\mathrm{T}}$ to be the normalized fundamental matrix solution of the *adjoint equation of variations*

$$\dot{\boldsymbol{\eta}} = -\left[\boldsymbol{\nabla}\mathbf{v}(\mathbf{x}(t; t_0, \mathbf{x}_0), t)\right]^{\mathrm{T}}\boldsymbol{\eta}, \tag{2.48}$$

whose solutions can, therefore, be written as

$$\boldsymbol{\eta}(t) = \left[\boldsymbol{\nabla}\mathbf{F}_{t_0}^{t}(\mathbf{x}_0)\right]^{-\mathrm{T}}\boldsymbol{\eta}_0 = \left[\boldsymbol{\nabla}\mathbf{F}_{t}^{t_0}(\mathbf{x}_0)\right]^{\mathrm{T}}\boldsymbol{\eta}_0. \tag{2.49}$$

By *Abel's theorem* for fundamental matrix solutions of linear differential equations (see Chicone, 2006), we conclude from Eq. (2.45) that

$$\det \boldsymbol{\nabla}\mathbf{F}_{t_0}^{t}(\mathbf{x}_0) = \exp\int_{t_0}^{t} \boldsymbol{\nabla}\cdot\mathbf{v}(\mathbf{x}(s; t_0, \mathbf{x}_0), s)\,ds. \tag{2.50}$$

Evaluating the general solution (2.46) requires knowledge of the deformation gradient, which is typically only available numerically. An exception is the case of *directionally steady velocity fields* $\mathbf{v}(\mathbf{x}, t)$, defined as

$$\dot{\mathbf{x}} = \mathbf{v}(\mathbf{x}, t) = \alpha(t)\mathbf{v}^0(\mathbf{x}) \tag{2.51}$$

for some nonzero, scalar-valued function $\alpha(t)$ of time and a steady velocity field $\mathbf{v}^0(\mathbf{x})$, whose flow map we denote by $\mathcal{F}_{t_0}^{t}$. By direct substitution, we find that the flow map of the ODE (2.51) is given by

$$\mathbf{F}_{t_0}^{t} = \mathcal{F}_{t_0}^{\int_{t_0}^{t}\alpha(s)\,ds}. \tag{2.52}$$

Then, for any directionally steady velocity field $\mathbf{v}(\mathbf{x}, t)$, an explicit solution of its equation of variations (2.45) is given by the *scaled Lagrangian velocity*

$$\boldsymbol{\xi}_1(t) = \mathbf{v}^0\left(\mathbf{F}_{t_0}^{t}(\mathbf{x}_0)\right). \tag{2.53}$$

Applying the general solution formula (2.46) for the equation of variations to the specific solution (2.53) gives the identity

$$\mathbf{v}^0\left(\mathbf{F}_{t_0}^{t}(\mathbf{x}_0)\right) = \boldsymbol{\nabla}\mathbf{F}_{t_0}^{t}(\mathbf{x}_0)\,\mathbf{v}^0(\mathbf{x}_0), \tag{2.54}$$

https://doi.org/10.1017/9781009225199.003 Published online by Cambridge University Press

where the flow map $\mathbf{F}_{t_0}^t$ is computable from formula (2.52) if the steady flow map $\mathcal{F}_{t_0}^t$ of $\mathbf{v}^0(\mathbf{x})$ is known.

For steady flows $\left(\alpha(t) \equiv 1 \text{ and hence } \mathbf{F}_{t_0}^t \equiv \mathcal{F}_{t_0}^t\right)$, a comparison of Eqs. (2.46) and (2.53) gives

$$\mathbf{v}\left(\mathbf{x}(t;\mathbf{x}_0)\right) = \nabla \mathbf{F}_{t_0}^t\left(\mathbf{x}_0\right)\mathbf{v}\left(\mathbf{x}_0\right), \tag{2.55}$$

confirming that the *Lagrangian velocity*

$$\mathbf{v}(t;\mathbf{x}_0) := \mathbf{v}\left(\mathbf{x}\left(t;t_0,\mathbf{x}_0\right),t\right) \tag{2.56}$$

is a solution of the equation of variations for any steady flow. In other words, the Lagrangian velocity $\mathbf{v}(t;\mathbf{x}_0)$ evolves as a material element in steady flows. For 2D steady flows, formula (2.55) leads to an explicit expression for the general solution (2.46) (see Haller and Iacono, 2003).

The equation of variations (2.45) is generally nonautonomous: it is an explicitly time-dependent system of linear differential equations, even if $\mathbf{v}$ is steady. As a consequence, the matrix $\nabla \mathbf{F}_{t_0}^t\left(\mathbf{x}_0\right)$ appearing in the solution (2.46) of this system is generally not a matrix exponential.[8] Accordingly, the eigenvalues of the matrix $\nabla \mathbf{v}(\mathbf{x}\left(t;t_0,\mathbf{x}_0\right),t)$, or of its time integral, $\int_{t_0}^t \nabla \mathbf{v}(\mathbf{x}\left(s;t_0,\mathbf{x}_0\right),s)\,ds$, have *no relevance* for the stability of the trivial solution $\boldsymbol{\xi} \equiv \mathbf{0}$ of this system (Verhulst, 2000). More generally, there is no systematic recipe available for solving nonautonomous linear ODEs: the eigenvalues and eigenvectors of their coefficient matrices have no general relationship to the solutions of these systems, which typically have to be found numerically. Example 2.1 illustrates this point for a planar Navier–Stokes velocity field.

Example 2.1 Consider the spatially linear velocity field

$$\dot{\mathbf{x}} = \mathbf{v}(\mathbf{x},t) = \mathbf{A}(t)\mathbf{x}, \qquad \mathbf{A}(t) = \begin{pmatrix} \sin 4t & \cos 4t + 2 \\ \cos 4t - 2 & -\sin 4t \end{pmatrix}, \tag{2.57}$$

which solves the planar, incompressible Navier–Stokes equation for any Reynolds number (Haller, 2005, 2015). The corresponding stream function is

$$\psi(\mathbf{x},t) = \frac{1}{2}\left(\cos 4t + 2\right)x_2^2 - \frac{1}{2}\left(\cos 4t - 2\right)x_1^2 + \frac{1}{2}x_1 x_2 \sin 4t, \tag{2.58}$$

whose instantaneous level curves at three different times are shown in the upper subplots of Fig. 2.11.

Along any trajectory $\mathbf{x}\left(t;t_0,\mathbf{x}_0\right)$ of this velocity field, the equation of variations (2.45) coincides with the velocity field:

$$\dot{\boldsymbol{\xi}} = \nabla \mathbf{v}(\mathbf{x}\left(t;t_0,\mathbf{x}_0\right),t)\boldsymbol{\xi} = \mathbf{A}(t)\boldsymbol{\xi}. \tag{2.59}$$

The eigenvalues of the coefficient matrix of this linear ODE are $\lambda_{1,2} = \pm i\sqrt{5}$, independent of the time t. By an ill-conceived analogy with the stability theory of autonomous linear ODEs, one could conclude that the $\boldsymbol{\xi} = 0$ solution of (2.59) is a center-type, neutrally stable fixed

[8] A rare exception is when the matrix $\nabla \mathbf{v}(\mathbf{x}\left(t;t_0,\mathbf{x}_0\right),t)$ commutes with $\int_{t_0}^t \nabla \mathbf{v}(\mathbf{x}\left(s;t_0,\mathbf{x}_0\right),s)\,ds$ (see Epstein, 1963). This happens, for instance, when $\nabla \mathbf{v}(\mathbf{x}\left(t;t_0,\mathbf{x}_0\right),t)$ is a diagonal matrix for a 2D or a 3D flow, or a skew-symmetric matrix for a 2D flow.

https://doi.org/10.1017/9781009225199.003 Published online by Cambridge University Press

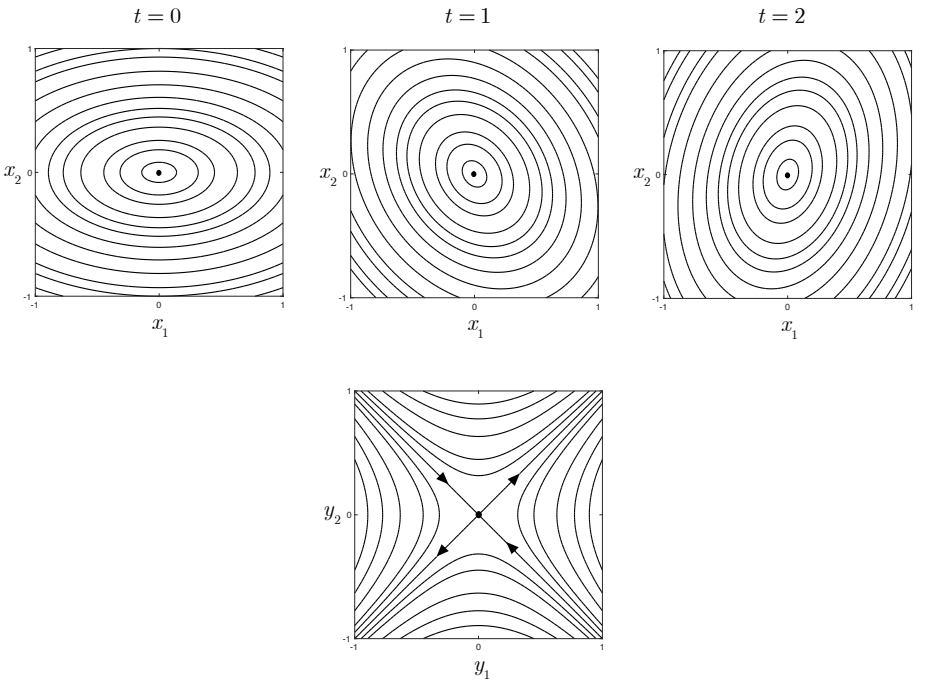

Figure 2.11 (Top) Streamlines obtained from the stream function (2.58) at three different time instances in the original **x**-frame. (Bottom) Streamlines marking actual trajectories of the same flow in the **y**-frame in which the velocity field becomes steady.

point, and hence all trajectories of Eq. (2.57) are neutrally stable, including its fixed point at $\mathbf{x} = \mathbf{0}$. However, passing to a rotating **y**-frame via the transformation

$$\mathbf{x} = \mathbf{T}(t)\mathbf{y}, \qquad \mathbf{T}(t) = \begin{pmatrix} \cos 2t & -\sin 2t \\ \sin 2t & \cos 2t \end{pmatrix},$$

transforms the velocity field (2.57) to the form

$$\dot{\mathbf{y}} = \mathbf{T}^{-1}\left[\mathbf{A}\mathbf{T} - \dot{\mathbf{T}}\right]\mathbf{y} = \begin{pmatrix} 0 & 1 \\ 1 & 0 \end{pmatrix}\mathbf{y}, \tag{2.60}$$

which is an autonomous, homogeneous linear system of ODEs. This system is explicitly solvable and the eigenvalues $\lambda_{1,2} = \pm 1$ of the time-independent coefficient matrix in Eq. (2.60) gives the correct characterization of the stability of the $\mathbf{y} = \mathbf{0}$ fixed point: it is a saddle-type fixed point and hence is unstable, as shown in the lower subplot of Fig. 2.11.

2.2.9 When Are the Eigenvalues of $\nabla\mathbf{v}$ Relevant?

As Example 2.1 illustrates, even if the eigenvalues of a nonautonomous linear system of ODEs – such as Eqs. (2.57) and (2.59) – are constant in time, these eigenvalues generally have no relationship to the solutions or the stability type of the ODE.

https://doi.org/10.1017/9781009225199.003 Published online by Cambridge University Press

An exception to this general rule is when the explicit time-dependence of $\boldsymbol{\nabla}\mathbf{v}(\mathbf{x}(t;t_0,\mathbf{x}_0),t)$ is slow enough (see, e.g., Haller, 2000; Haller and Iacono, 2003). In that case, a linear transformation $\boldsymbol{\xi} = \mathbf{T}(t)\boldsymbol{\eta}$ to the time-evolving eigenbasis of $\boldsymbol{\nabla}\mathbf{v}(\mathbf{x}(t;t_0,\mathbf{x}_0),t)$ can be constructed when such an eigenbasis exists, with $\mathbf{T}(t)$ containing the unit eigenvectors of $\boldsymbol{\nabla}\mathbf{v}(\mathbf{x}(t;t_0,\mathbf{x}_0),t)$. As in Example 2.1, this transformation puts the equation of variations (2.45) in the form

$$\begin{aligned}\dot{\boldsymbol{\eta}} &= \mathbf{T}^{-1}(t)\left[\boldsymbol{\nabla}\mathbf{v}(\mathbf{x}(t;t_0,\mathbf{x}_0),t)\mathbf{T}(t) - \dot{\mathbf{T}}(t)\right]\boldsymbol{\eta} \\ &= \left[\boldsymbol{\Lambda}(t) + \mathbf{T}^{-1}(t)\dot{\mathbf{T}}(t)\right]\boldsymbol{\eta},\end{aligned} \tag{2.61}$$

where $\boldsymbol{\Lambda}(t)$ is a diagonal matrix that contains the time-dependent eigenvalues of $\boldsymbol{\nabla}\mathbf{v}(\mathbf{x}(t;t_0,\mathbf{x}_0),t)$. If $\boldsymbol{\nabla}\mathbf{v}(\mathbf{x}(t;t_0,\mathbf{x}_0),t)$ is slowly varying, then $\dot{\mathbf{T}}(t)$ is small in norm and hence the solutions of (2.61) remain close to those of the diagonalized system $\dot{\boldsymbol{\eta}} = \boldsymbol{\Lambda}(t)\boldsymbol{\eta}$ for some time. The latter system is explicitly solved by $\boldsymbol{\eta}(t) = \left[\exp\int_{t_0}^{t}\boldsymbol{\Lambda}(s)\,ds\right]\boldsymbol{\eta}(t_0)$, which shows that the time-integrated eigenvalues $\boldsymbol{\nabla}\mathbf{v}(\mathbf{x}(t;t_0,\mathbf{x}_0),t)$ determine the stability of the $\boldsymbol{\eta} = \mathbf{0}$ fixed point of Eq. (2.61), and hence the linearized stability of the underlying trajectory $\mathbf{x}(t;t_0,\mathbf{x}_0)$ for some finite time. However, the slow-variation assumption on $\boldsymbol{\nabla}\mathbf{v}(\mathbf{x}(t;t_0,\mathbf{x}_0),t)$ leading to this conclusion will, in general, be violated even in steady flows. Indeed, along a nonequilibrium trajectory $\mathbf{x}(t;t_0,\mathbf{x}_0)$ of a steady velocity field $\mathbf{v}(\mathbf{x})$, the velocity gradient $\boldsymbol{\nabla}\mathbf{v}(\mathbf{x}(t;t_0,\mathbf{x}_0))$ will, in general, be highly unsteady.

In contrast, if the velocity field $\mathbf{v}$ is steady *and* has a fixed point at $\mathbf{p}$, then the equation of variations (2.45) along the trajectory $\mathbf{x}(t;t_0,\mathbf{p}) \equiv \mathbf{p}$ is the autonomous ODE

$$\dot{\boldsymbol{\xi}} = \boldsymbol{\nabla}\mathbf{v}(\mathbf{p})\boldsymbol{\xi}, \tag{2.62}$$

which is solved by

$$\boldsymbol{\xi}(t) = \boldsymbol{\nabla}\mathbf{F}^{t}(\mathbf{p})\,\boldsymbol{\xi}_0 = e^{\boldsymbol{\nabla}\mathbf{v}(\mathbf{p})t}\boldsymbol{\xi}_0. \tag{2.63}$$

In this case, therefore, the fundamental matrix solution of the equation of variations is a matrix exponential and hence the eigenvalues and eigenvectors of the velocity Jacobian $\boldsymbol{\nabla}\mathbf{v}(\mathbf{p})$ correctly determine the linearized flow geometry near $\mathbf{p}$. Therefore, the linearized streamline geometries we showed in Figs. 2.2 and 2.5 coincide with actual linearized fluid trajectory patterns near stagnation points of steady flows.

2.2.10 Lagrangian Aspects of the Vorticity

Taking the curl of both sides of the incompressible Euler equation (2.16) and using some classic vector identities gives the *inviscid vorticity transport equation*

$$\frac{D\boldsymbol{\omega}}{Dt} = (\boldsymbol{\nabla}\mathbf{v})\,\boldsymbol{\omega}, \tag{2.64}$$

where $\frac{D(\cdot)}{Dt} = \partial_t(\cdot) + \boldsymbol{\nabla}(\cdot)\,\mathbf{v}$ denotes the *material derivative,* the derivative of a quantity $(\cdot)$ along trajectories of the velocity field $\mathbf{v}$. Along a trajectory $\mathbf{x}(t;t_0,\mathbf{x}_0)$, the linear system of ODEs (2.64) coincides with the equations of variations (2.45). Therefore, we must have

$$\boldsymbol{\omega}(\mathbf{x}(t;t_0,\mathbf{x}_0),t) = \boldsymbol{\nabla}\mathbf{F}_{t_0}^{t}(\mathbf{x}_0)\,\boldsymbol{\omega}(\mathbf{x}_0,t_0), \tag{2.65}$$

https://doi.org/10.1017/9781009225199.003 Published online by Cambridge University Press

which means that the vorticity vector along a trajectory of an inviscid flow evolves as a material element advected by the linearized flow along the same trajectory. The same conclusion does not hold for viscous flows, because the *viscous vorticity transport equation*,

$$\frac{D\boldsymbol{\omega}}{Dt} = (\boldsymbol{\nabla}\mathbf{v})\,\boldsymbol{\omega} + \nu\boldsymbol{\Delta}\boldsymbol{\omega}, \tag{2.66}$$

obtained through the same steps form the Navier–Stokes equation

$$\partial_t\mathbf{v} + (\boldsymbol{\nabla}\mathbf{v})\,\mathbf{v} = -\frac{1}{\rho}\nabla p + \nu\boldsymbol{\Delta}\mathbf{v} + \mathbf{g}, \tag{2.67}$$

with pressure p, density ρ, viscosity ν and constant of gravity $\mathbf{g}$, contains the additional term $\nu\boldsymbol{\Delta}\boldsymbol{\omega}$ compared to the equation of variations. Using the variation of constants formula for inhomogeneous linear systems of ODEs, we obtain

$$\boldsymbol{\omega}\left(\mathbf{x}(t;t_0,\mathbf{x}_0),t\right) = \boldsymbol{\nabla}\mathbf{F}_{t_0}^{t}\left(\mathbf{x}_0\right)\boldsymbol{\omega}\left(\mathbf{x}_0,t_0\right) + \nu\int_{t_0}^{t}\boldsymbol{\nabla}\mathbf{F}_{s}^{t}\left(\mathbf{x}(s;t_0,\mathbf{x}_0)\right)\boldsymbol{\Delta}\boldsymbol{\omega}\left(\mathbf{x}(s;t_0,\mathbf{x}_0),s\right)\,ds.$$

This expression is not explicit for $\boldsymbol{\omega}$, but shows that the non-material nature of the vorticity is governed by the integral of the materially advected vorticity Laplacian, multiplied by the viscosity.

For 2D flows with a velocity field $\mathbf{v}(\mathbf{x}) = (u(x,y), v(x,y), 0)$, the vorticity vector takes the form $\boldsymbol{\omega} = (0,0,\omega_z)$, with $\omega_z(\mathbf{x}) = \omega_z(x,y)$ denoting its z-component. In that case, only the z-component of Eq. (2.66) is nonzero, yielding the 2D vorticity transport equation as a scalar advection–diffusion equation

$$\frac{D\omega_z}{Dt} = \nu\Delta\omega_z. \tag{2.68}$$

Accordingly, for inviscid flows ($\nu = 0$), we obtain the conservation law

$$\frac{D\omega_z}{Dt} = \partial_t\omega_z + \boldsymbol{\nabla}\omega_z\cdot\mathbf{v} = 0. \tag{2.69}$$

This means that the scalar vorticity is preserved along the trajectories of 2D incompressible flows.

Taking the gradient of Eq. (2.69) then gives

$$\partial_t\left(\boldsymbol{\nabla}\omega_z\right) + \boldsymbol{\nabla}\left(\boldsymbol{\nabla}\omega_z\right)\mathbf{v} = -\left(\boldsymbol{\nabla}\mathbf{v}\right)^{\mathrm{T}}\boldsymbol{\nabla}\omega_z, \tag{2.70}$$

or, equivalently,

$$\frac{D}{Dt}\boldsymbol{\nabla}\omega_z = -\left(\boldsymbol{\nabla}\mathbf{v}\right)^{\mathrm{T}}\boldsymbol{\nabla}\omega_z. \tag{2.71}$$

This shows that the vorticity gradient along trajectories satisfies the adjoint equation of variations (2.48). Therefore, the adjoint solution formula (2.49) implies that the vorticity gradient along a trajectory $\mathbf{x}(t;t_0,\mathbf{x}_0)$ of a planar inviscid flows evolves according to the formula

$$\boldsymbol{\nabla}\omega_z\left(\mathbf{x}(t;t_0,\mathbf{x}_0),t\right) = \left[\boldsymbol{\nabla}\mathbf{F}_{t_0}^{t}\left(\mathbf{x}_0\right)\right]^{-\mathrm{T}}\boldsymbol{\nabla}\omega_z\left(\mathbf{x}_0,t_0\right). \tag{2.72}$$

https://doi.org/10.1017/9781009225199.003 Published online by Cambridge University Press

2.2.11 Dynamics Near Fixed Points of Steady Flows

We now discuss the implications of the linearized stability type of a fixed point $\mathbf{p}$ of a steady velocity field $\mathbf{v}(\mathbf{x})$ (see Eq. (2.62)) for nearby fluid trajectories. We call $\mathbf{p}$ a *hyperbolic fixed point* if $\mathrm{Re}\,\lambda_i \neq 0$ holds for all eigenvalues λ_i of the matrix $\nabla\mathbf{v}(\mathbf{p})$.

By the *Hartman–Grobman theorem* (see Guckenheimer and Holmes, 1983), autonomous dynamical systems are locally topologically conjugate to their linearization near hyperbolic fixed points. This means that locally near $\mathbf{p}$, there exists a continuous and continuously invertible change of coordinates $\mathbf{x} = \mathbf{h}(\boldsymbol{\xi})$ that transforms the trajectories of the velocity field $\mathbf{v}(\mathbf{x})$ into those of $\nabla\mathbf{v}(\mathbf{p})\boldsymbol{\xi}$, preserving the parametrization of orbits by time.[9] Any robust nonlinear trajectory pattern near an off-boundary fixed point is, therefore, a small deformation of one of the hyperbolic instantaneous streamline patterns shown in Fig. 2.2 and Fig. 2.5.

A notable nonhyperbolic fixed point in steady incompressible flows is one with a pair of purely imaginary eigenvalues. In 2D steady flows, the linearized Lagrangian dynamics at such an *elliptic fixed point* (see Fig. 2.2) nevertheless correctly represent nearby trajectory patterns of the full flow, although the Hartman–Grobman theorem is formally inapplicable to such a fixed point.[10] In 3D, steady incompressible flows, nonhyperbolic fixed points are those where $\nabla\mathbf{v}$ has either three zero eigenvalues or a purely imaginary pair and a zero eigenvalue. For such fixed points, further analysis is needed beyond the linearization to understand the local geometry of material trajectories.

Another frequent type of nonhyperbolic fixed point in steady flows is any point on a no-slip boundary. In two dimensions, such boundary points occur along a parametrized curve $\boldsymbol{\gamma}(s)$, implying $\mathbf{v}(\boldsymbol{\gamma}(s)) \equiv \mathbf{0}$. Differentiating this equation with respect to s and invoking the chain rule, we obtain that $\nabla\mathbf{v}(\boldsymbol{\gamma}(s))$ must have a zero eigenvalue for each s, corresponding to the eigenvector $\boldsymbol{\gamma}'(s)$. Incompressibility then implies the other eigenvalue of $\nabla\mathbf{v}(\boldsymbol{\gamma}(s))$ to be zero as well, as we indicated for degenerate parabolic stagnation points in Fig. 2.2. One can, however, remove this degeneracy from the equation of motion $\dot{\mathbf{x}} = \mathbf{v}(\mathbf{x})$ by introducing the new time τ via the relation $d\tau/dt = y(t)$, with $y(t)$ denoting the boundary-normal component of trajectories (see Haller, 2004 and Surana et al., 2006). After this rescaling, the fixed points along the no-slip boundary typically disappear or become hyperbolic fixed points, as we noted for instantaneous stagnation points in §2.1.3 (see Fig. 2.5).

2.2.12 Poincaré Maps

Here we discuss how flows generated by temporally recurrent velocity fields can be analyzed in a simpler fashion through stroboscopic images of evolving fluid particles.

[9] More specifically, in a small enough, open neighborhood $U \subset \mathbb{R}^n$ of the fixed point $\mathbf{p}$, we have $e^{\nabla\mathbf{v}(\mathbf{p})t}\mathbf{h}^{-1}(\mathbf{x}_0) = \mathbf{h}^{-1}(\mathbf{F}^t(\mathbf{x}_0))$ for all initial conditions $\mathbf{x}_0 \in U$ and for all times t satisfying $\mathbf{F}^t(\mathbf{x}_0) \in U$.

[10] This conclusion follows from the application of Lyapunov's second method (see, e.g., Rouche et al., 1977, Chicone, 2006) for stability analysis if one chooses the stream function $\psi(\mathbf{x})$ as a Lyapunov function. This Lyapunov function has a local minimum or maximum at elliptic fixed points, which are encircled by closed streamlines in this case. By Eq. (2.5), the Lyapunov function $\psi(\mathbf{x})$ is also constant along trajectories, implying the stability of the elliptic fixed point by Lyapunov's classic stability theorem.

Time-Periodic Flows

An important special class of flows is generated by time-periodic velocity fields. Trajectories of such flows satisfy an ODE of the specific form

$$\dot{\mathbf{x}} = \mathbf{v}(\mathbf{x}, t), \quad \mathbf{v}(\mathbf{x}, t) = \mathbf{v}(\mathbf{x}, t + T), \tag{2.73}$$

for some time period $T > 0$, for $\mathbf{x} \in \mathbb{R}^n$ with $n = 2$ or $n = 3$. The evolution rule for trajectories, therefore, repeats itself periodically in time, enabling a simplified study of the discretized evolution of trajectories over time intervals that are integer multiples of T.

Specifically, the *Poincaré map* (or period T-map), denoted $\mathbf{P}_{t_0}$, of the ODE (2.73) is the restriction of its flow map to one time period starting at time t_0:

$$\mathbf{P}_{t_0} := \mathbf{F}_{t_0}^{t_0+T}. \tag{2.74}$$

We illustrate this definition for 2D flows in Fig. 2.12.

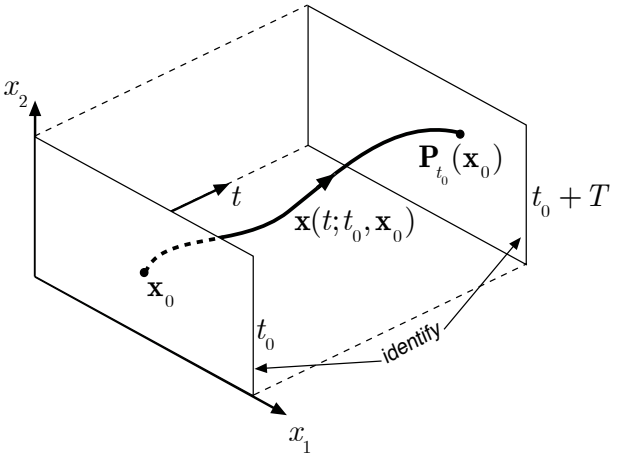

Figure 2.12 The definition of the Poincaré map $\mathbf{P}_{t_0}$ for a 2D velocity field whose time dependence is T-periodic.

By the time-periodicity of the ODE (2.73), the flow map advancing particle positions between times $t_0 + jT$ and $t_0 + (j + 1)T$ is the same map for any integer j. Therefore, by the group property of flow maps (see Eq. (2.24)), the repeated iteration of the single mapping $\mathbf{P}_{t_0}$ gives the fluid particle positions at forward and backward times that are separated from t_0 by an integer multiple of T:

$$\mathbf{F}_{t_0}^{t_0+kT} = \mathbf{F}_{t_0+(k-1)T}^{t_0+kT} \circ \cdots \circ \mathbf{F}_{t_0}^{t_0+T} = \underbrace{\mathbf{P}_{t_0} \circ \cdots \circ \mathbf{P}_{t_0}}_{k} = \mathbf{P}_{t_0}^k(\mathbf{x}_0).$$

The infinite set of iterations $\left\{\mathbf{x}_0, \mathbf{P}_{t_0}(\mathbf{x}_0), \mathbf{P}_{t_0}^2(\mathbf{x}_0), \ldots, \mathbf{P}_{t_0}^k(\mathbf{x}_0), \ldots\right\}$ is called the *orbit of* $\mathbf{P}_{t_0}$ starting from the point $\mathbf{x}_0$. We also note the relation

$$\mathbf{P}_{t_1} = \mathbf{F}_{t_1}^{t_1+T} = \mathbf{F}_{t_0+T}^{t_1+T} \circ \mathbf{F}_{t_0}^{t_0+T} \circ \mathbf{F}_{t_1}^{t_0} = \mathbf{F}_{t_0}^{t_1} \circ \mathbf{P}_{t_0} \circ \mathbf{F}_{t_1}^{t_0} = \left(\mathbf{F}_{t_1}^{t_0}\right)^{-1} \circ \mathbf{P}_{t_0} \circ \mathbf{F}_{t_1}^{t_0}, \tag{2.75}$$

which shows that Poincaré maps based at any two different times, t_0 and t_1, are always *topologically conjugate*. Such maps share the same orbit structure up to the smooth deformation

https://doi.org/10.1017/9781009225199.003 Published online by Cambridge University Press

represented by $\mathbf{F}_{t_1}^{t_0}$ (see Guckenheimer and Holmes, 1983). Topological conjugacy is a stronger form of the notion of topological equivalence introduced in §2.2.7: it does not allow for a reparametrization of time (i.e., $\tau(\mathbf{x}_0, t) \equiv t$ must hold).

The computation of the Poincaré map for a general 2D, time-periodic velocity field is implemented in Notebook 2.1.

Notebook 2.1 (`PoincareMap2D`) *Computes the Poincaré map defined for a 2D, time-periodic velocity data set.*
https://github.com/haller-group/TBarrier/tree/main/TBarrier/2D/demos/AdvectiveBarriers/PoincareMap2D

If $\mathbf{v}(\mathbf{x}, t)$ is divergence-free, then the flow map is volume-preserving (see condition (2.40)) and so is the Poincaré map

$$\det \boldsymbol{\nabla} \mathbf{P}_{t_0} = 1, \qquad \text{vol}\left(\mathbf{P}_{t_0}(V)\right) = \text{vol}\,(V) \tag{2.76}$$

for any set $V \subset U$. For an incompressible time-periodic flow, the volume-preservation of its Poincaré map has important global consequence on the dynamics, which we will discuss in §§2.2.13–2.2.14.

While we will discuss the power of Poincaré maps in later chapters, Fig. 2.13 shows a preliminary illustration of their usefulness. The figure shows experimentally observed mixing patterns whose transport barriers (or lack thereof) are revealed by Poincaré maps computed from trajectories of the corresponding model velocity fields.

Quasiperiodic Flows

Quasiperiodic time-dependence in a velocity field can be represented by rewriting the general particle equation of motion (2.17) as

$$\dot{\mathbf{x}} = \mathbf{v}(\mathbf{x}, \Omega_1 t, \ldots, \Omega_m t), \qquad \mathbf{x} \in \mathbb{R}^n, \quad t \in \mathbb{R}, \tag{2.77}$$

with a velocity field $\mathbf{v}$ whose time-dependence involves several frequencies, Ω_j, not just one.[11] We assume that the frequencies Ω_j are *rationally independent*, which means that the frequency vector $\boldsymbol{\Omega} = (\Omega_1, \ldots, \Omega_m)$ satisfies

$$\langle \boldsymbol{\Omega}, \mathbf{k} \rangle \neq 0 \tag{2.78}$$

for all integer vectors $\mathbf{k} \in \mathbb{Z}^m$. If the frequencies were not rationally independent, then one could select a smaller number of Ω_j frequencies to represent the velocity field (2.77).

We can turn system (2.77) into a temporally periodic, higher-dimensional dynamical system by introducing the phase vector $\boldsymbol{\phi} = (\phi_2, \ldots, \phi_m)$ with the individual phases $\phi_j = \Omega_j t$ for $j = 2, \ldots, m$. We view this phase vector as an element of an $(m-1)$-*dimensional torus*

$$\mathbb{T}^{m-1} = \underbrace{S^1 \times \cdots \times S^1}_{m-1}, \tag{2.79}$$

[11] Time periodic flows ($m = 1$) also fall in this general family.

https://doi.org/10.1017/9781009225199.003 Published online by Cambridge University Press

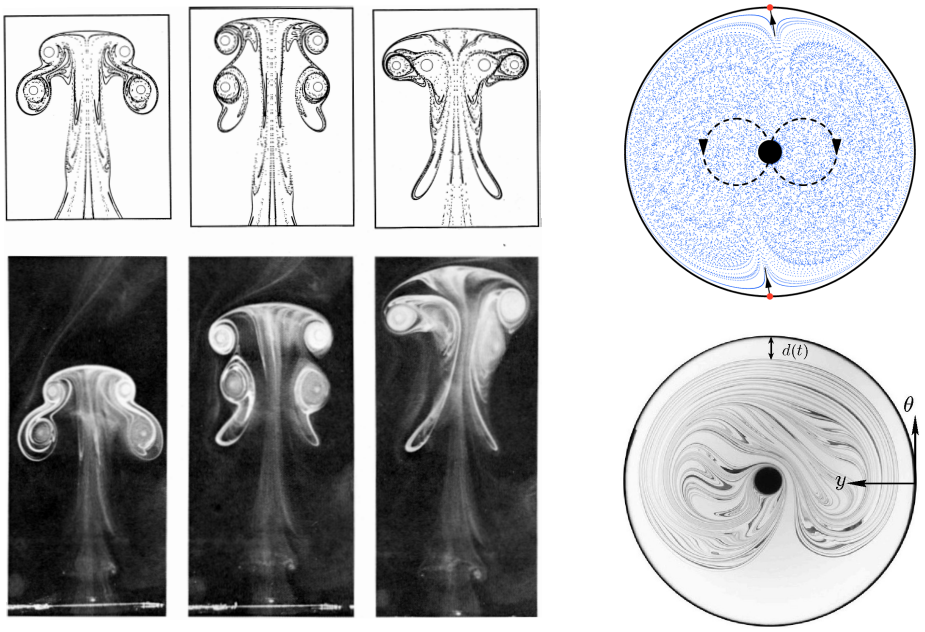

Figure 2.13 (Bottom) Dye visualization vs. (top) Poincaré maps for two time-periodic flows. (a) Leapfrogging vortex pair visualized by smoke (reproduced from Shariff et al., 2006, who used the experimental photographs of Yamada and Matsui, 1978). (b) Experiment involving a moving mixer rod in sugar syrup. The figure-of-eight path of the mixing rod is shown in the upper Poincaré maps, which were computed numerically from a single trajectory of a model flow. An upper and a lower stagnation point is shown in red. Adapted from Thiffeault et al. (2011).

i.e., the $(m-1)$-fold topological product of the unit circle S^1 with itself. We can now rewrite system (2.17) as

$$\begin{aligned} \dot{\mathbf{x}} &= \mathbf{v}(\mathbf{x}, \Omega_1 t, \boldsymbol{\phi}), \\ \dot{\boldsymbol{\phi}} &= \begin{pmatrix} \Omega_2 \\ \vdots \\ \Omega_m \end{pmatrix}, \end{aligned} \tag{2.80}$$

a time-periodic dynamical system on the $(n+m-1)$-dimensional phase space $\mathbb{R}^n \times \mathbb{T}^{m-1}$ with period $T = 2\pi/\Omega_1$.

Only some of the trajectories of the extended dynamical system (2.80) will, however, represent trajectories of the ODE (2.17). Indeed, while one can formally select an arbitrary initial phase vector $\boldsymbol{\phi}(t_0)$ as initial condition in the ODE (2.80), the phase variables $(\Omega_2 t, \ldots, \Omega_m t)$ in the original system (2.77) are constrained to evolve together from the initial vector

$$\boldsymbol{\phi}_0 = (\Omega_2 t_0, \ldots, \Omega_m t_0)\,. \tag{2.81}$$

https://doi.org/10.1017/9781009225199.003 Published online by Cambridge University Press

Therefore, the elements of this vector cannot be selected arbitrarily relative to each other and relative to the first phase variable $\Omega_1 t_0$. For this reason, only an $(n+1)$-dimensional family of initial conditions of the $(n+m-1)$-dimensional system (2.80) are relevant for the original system (2.17).[12]

This relevant set of initial conditions is a dense set in the $(n+m-1)$-dimensional phase space because the curve of initial conditions satisfying Eq. (2.81) forms a dense curve in the torus $\mathbb{T}^{m-1}$ due to the assumed rational independence of the frequencies $(\Omega_2, \ldots, \Omega_m)$. This dense set, however, has *measure zero* within the torus: it can be covered by a countable set of open subsets of the torus that have arbitrarily small total volume (total length for $m = 2$ and total area for $m = 3$). As a consequence, the trajectories of the extended system (2.80) that are related to the original quasiperiodic velocity field $\mathbf{v}(\mathbf{x}, \boldsymbol{\Omega} t)$ form a measure zero set in the phase space of Eq. (2.80). As a consequence, mathematical statements obtained for almost all (i.e., all but a measure zero set of) trajectories of the extended system (2.80) do not carry over to the original quasiperiodic velocity field (2.77). Examples of such statements are the Poincaré recurrence theorem (§2.2.13) and Birkhoff's ergodic theorem (§2.2.14).

For the extended system (2.80), we can define a Poincaré map in the same way as for the time-periodic system (2.73). Indeed, for any fixed initial time t_0 and for the time period $T = 2\pi/\Omega_1$, an *extended Poincaré map* $\mathbf{P}_{t_0}$ can be defined on the space $\mathbb{R}^n \times \mathbb{T}^{m-1}$ as

$$\begin{aligned} &\mathbf{P}_{t_0} : \mathbb{R}^n \times \mathbb{T}^{m-1} \to \mathbb{R}^n \times \mathbb{T}^{m-1}, \\ &(\mathbf{x}_0, \phi_{20}, \ldots, \phi_{m0}) \mapsto (\mathbf{x}(t_0 + T; t_0, \mathbf{x}_0, \Omega_1 t_0, \boldsymbol{\phi}_0), \phi_{20} + \Omega_2 T, \ldots, \phi_{m0} + \Omega_m T). \end{aligned} \tag{2.82}$$

We sketch the geometry of this Poincaré map for 2D flows ($n = 2$) in Fig. 2.14. Similar Poincaré maps can be defined based on any of the periods $T_j = 2\pi/\Omega_j$ associated with the remaining frequencies for $j = 2, \ldots, m$.

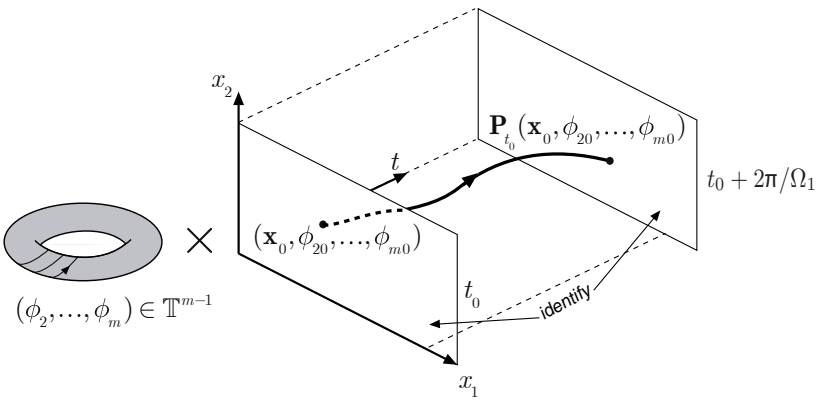

Figure 2.14 The definition of the Poincaré map $\mathbf{P}_{t_0}$ for a 2D, temporally quasiperiodic velocity field with m rationally independent frequencies.

By our discussion in §2.2.12, the Poincaré map $\mathbf{P}_{t_0}$ defined for the extended system (2.80) is volume preserving precisely when the velocity field $\mathbf{v}$ is incompressible. As we noted for the extended flow (2.80), only a dense but measure zero set of orbits of the Poincaré

[12] This restriction leads to conservation laws in the phase space of system (2.80), as we will see in §4.3.2.

https://doi.org/10.1017/9781009225199.003 Published online by Cambridge University Press

$\mathbf{P}_{t_0}$ correspond to sampled fluid trajectories of the original vector quasiperiodic vector field (2.77). Such a dense set of admissible trajectories of $\mathbf{P}_{t_0}$ will give a good description of the overall behavior of the fluid but is still only a measure zero set.

3D Steady Flows

As we have already pointed out in the previous section, any steady flow can be considered time-periodic with any period. This enables the sampling of 3D steady flows with arbitrary stroboscopic maps. These sampling maps, however, are still 3D, so there is no immediate practical advantage from such a temporal discretization of the steady flow. However, there is an alternative way to construct Poincaré maps in 3D flows that does bring dimensional reduction, as we discuss next.

Consider a 2D surface $\Sigma \subset \mathbb{R}^3$ that is everywhere transverse (i.e., nontangent) to the velocity field $\mathbf{v}(\mathbf{x})$. For such a *Poincaré section* Σ, the *first-return map*, or *Poincaré map,* $\mathbf{P}_\Sigma : \Sigma \to \Sigma$ can then be defined as the mapping that takes an initial condition $\mathbf{x}_0 \in \Sigma$ into the first intersection of the trajectory starting from $\mathbf{x}_0$ with Σ, if such an intersection exists (see Fig. 2.15).

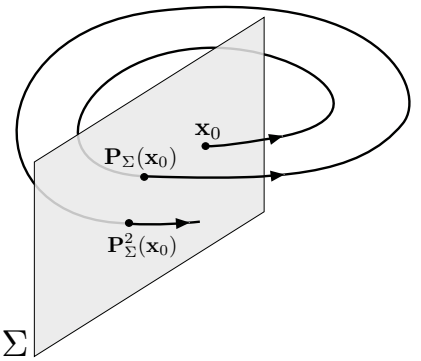

Figure 2.15 A Poincaré map (or first-return map) $\mathbf{P}_\Sigma$ and its second iterate, $\mathbf{P}_\Sigma^2$, defined on a section Σ transverse to a 3D, steady velocity field.

More specifically, using the flow map $\mathbf{F}^t$ of $\mathbf{v}$, we can write

$$\mathbf{P}_\Sigma(\mathbf{x}_0) := \mathbf{F}^{t_{\min}(\mathbf{x}_0)}(\mathbf{x}_0), \qquad t_{\min}(\mathbf{x}_0) = \min\left\{t > 0 \,:\, \mathbf{x}_0 \in \Sigma,\ \mathbf{F}^t(\mathbf{x}_0) \in \Sigma\right\}. \tag{2.83}$$

The computation of the Poincaré map for a general 3D steady velocity field is implemented in Notebook 2.2.

Notebook 2.2 (`PoincareMap3D`) *Computes the Poincaré map defined for a 3D steady velocity data set.*
https://github.com/haller-group/TBarrier/tree/main/TBarrier/3D/demos/AdvectiveBarriers/PoincareMap3D

If Σ and $\mathbf{v}$ are smooth and $\mathbf{n}_\Sigma(\mathbf{x})$ denotes a unit normal field along Σ with the orientation $\mathbf{v} \cdot \mathbf{n}_\Sigma > 0$,[13] then the Poincaré map $\mathbf{P}_\Sigma$ is a diffeomorphism that preserves the generalized area element

[13] It is always possible to choose such an orientation for the unit normal field $\mathbf{n}_\Sigma$ globally on Σ. This is because the

https://doi.org/10.1017/9781009225199.003 Published online by Cambridge University Press

$$d\tilde{A} = \mathbf{v} \cdot \mathbf{n}_\Sigma \, dA, \tag{2.84}$$

as we show in Appendix A.14. As a result, $\mathbf{P}_\Sigma$ is generally not area preserving but falls in the family of *symplectic maps*, defined as mappings that preserve a nondegenerate, closed two-form (see, e.g., Abraham et al., 1988). For any symplectic map, appropriate local coordinates can be constructed so that the map preserves the classic area element on Σ in the new coordinates (see Appendix A.14). Therefore, the classification of the linearized Poincaré map $\nabla \mathbf{P}_\Sigma(\mathbf{p})$ at a fixed point $\mathbf{p}$ on Σ is identical to that of the Poincaré map of a 2D, time-periodic flow (see Fig. 4.3). Global features of 2D symplectic maps coincide with those we already mentioned for area-preserving maps in §4.1 (see Mackay et al., 1984; Meiss, 1992).

Similarly, a first-return map $\mathbf{P}_\Sigma$ defined on a transverse cross section Σ of a compressible but mass-preserving, steady, 3D flow preserves the generalized area element

$$d\tilde{A} = \rho \mathbf{v} \cdot \mathbf{n}_\Sigma \, dA, \tag{2.85}$$

where $\rho(\mathbf{x}) > 0$ is the mass density field of the fluid (see Appendix A.14). Local and global qualitative properties of Poincaré maps in such flows, therefore, also coincide with those of period-T maps of time-periodic 2D flows.

2.2.13 Revisiting Initial Conditions: Poincaré's Recurrence Theorem

Assume that the Poincaré map $\mathbf{P}_{t_0}$ of a T-periodic velocity field $\mathbf{v}(\mathbf{x}, t)$ leaves a compact domain $D \subset U$ invariant, i.e., $\mathbf{P}_{t_0}(D) = D$ holds. This is the case, for instance, if the velocity field $\mathbf{v}$ is defined on a closed and bounded domain $D \equiv U$ surrounded by impenetrable boundaries. In such cases, *Poincaré's recurrence theorem* for measure-preserving maps (Arnold, 1989) guarantees that almost all orbits of $\mathbf{P}_{t_0}$ return arbitrarily close to their initial position $\mathbf{x}_0$ over long enough time intervals, as illustrated in Fig. 2.16. In other words, trajectories that do not return arbitrarily close to their initial positions over long times form a set of zero volume. Note that Poincaré's theorem also guarantees repeated returns to D occurring after an arbitrarily large threshold time t^*. This can be deduced by applying the theorem to the measure-preserving map $\tilde{\mathbf{P}}_{t_0} := \mathbf{P}_{t_0}^N$, with the positive integer N selected so that $NT > t^*$ holds.

Phrased in terms of the orbits of $\mathbf{v}(\mathbf{x}, t)$ in continuous time, almost all trajectories of a time-periodic incompressible flow defined on a closed and bounded domain revisit their initial conditions repeatedly with arbitrarily high accuracy over arbitrarily long times. Since steady flows can be considered periodic with any period, Poincaré's recurrence theorem applies to them as well. Remarkably, therefore, almost all trajectories of a steady incompressible flow confined to a closed and bounded 2D or 3D domain revisit their initial positions arbitrarily closely over arbitrary long times.

In its most general form, Poincaré's recurrence theorem only assumes the conservation of a measure (Arnold, 1989). As we have seen, compressible flows obeying the equation of continuity conserve mass (see formula (2.43)), which makes their Poincaré maps measure preserving. Therefore, almost all trajectories of a compressible but mass-preserving, steady

inner product $\mathbf{v} \cdot \mathbf{n}_\Sigma$ cannot vanish anywhere on Σ by the transversality of $\mathbf{v}$ to Σ, and hence this inner product cannot change sign on Σ.

https://doi.org/10.1017/9781009225199.003 Published online by Cambridge University Press

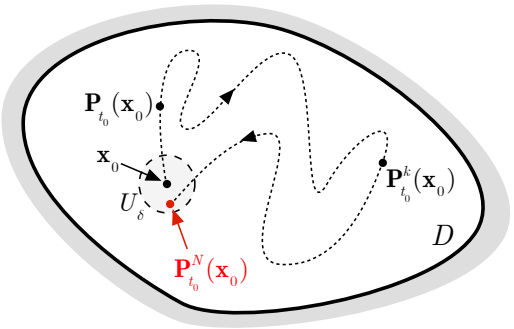

Figure 2.16 The statement of the Poincaré recurrence theorem applied to the Poincaré map $\mathbf{P}_{t_0}$ on a compact invariant domain D. Almost all (i.e., all but a measure zero set of) initial conditions $\mathbf{x}_0$ generate trajectories for $\mathbf{P}_{t_0}$ that return for some large enough iteration N of $\mathbf{P}_{t_0}$ to any small neighborhood U_δ of $\mathbf{x}_0$.

or time-periodic flow defined on a closed and bounded domain revisit their initial positions arbitrarily closely over arbitrarily long times.

At first sight, it might seem that Poincaré's recurrence theorem is also applicable to the quasiperiodic vector fields $\mathbf{v}(\mathbf{x}, \mathbf{\Omega}t)$ with frequency vector $\mathbf{\Omega} = (\Omega_1, \ldots, \Omega_m)$ discussed in §2.2.12. Indeed, if the original quasiperiodic velocity field (2.77) is defined on a compact invariant domain D, then the extended Poincaré map $\mathbf{P}_{t_0}$, introduced in formula (2.82), is defined on the compact set $D \times \mathbb{T}^m$, given that the m-dimensional torus, $\mathbb{T}^m$, is compact. This enables us to apply the Poincaré recurrence theorem to the extended map $\mathbf{P}_{t_0}$ and conclude that almost all trajectories $\mathbf{X}(t; \mathbf{X}_0) = (\mathbf{x}(t; \mathbf{x}_0), \phi_0 + \mathbf{\Omega}t)$ return arbitrarily close to $\mathbf{X}_0 = (\mathbf{x}_0, \phi_0)$ for large enough times t. Note, however, that Poincaré's recurrence theorem allows for the existence of a measure zero set of nonrecurrent trajectories in the phase space of the extended system (2.80). The trajectories in that extended phase space that correspond to actual trajectories of the original quasiperiodic velocity field (2.77) also form just a measure zero set. Therefore, for all we know from this argument, all trajectories of $\mathbf{v}(\mathbf{x}, \mathbf{\Omega}t)$ may be nonrecurrent. Consequently, recurrence in temporally quasiperiodic velocity fields does not follow from Poincaré's recurrence theorem.

The recurrence theorem, however, is applicable to Poincaré maps defined on transverse sections of 3D steady, volume-preserving or mass-preserving flows (see §2.2.12). Namely, on any compact spatial domain invariant under such a flow, typical trajectories will return to any Poincaré section that is transverse to the velocity field. This recurrence guarantees the existence of initial conditions arbitrarily close to Σ that will return to their arbitrarily small neighborhoods. These returning trajectories will, therefore, come back arbitrarily close to Σ over time and hence will have to intersect Σ at some point due to the transversality of the vector field $\mathbf{v}$ to Σ. The same argument in backward time guarantees that such trajectories also had an intersection with Σ at some point in the past, and hence these trajectories start from, and return to, Σ.

Poincaré's recurrence theorem, however, does not hold when the domain of definition D of the field (2.77) is not a bounded invariant set, or when the time-dependence of the velocity

https://doi.org/10.1017/9781009225199.003 Published online by Cambridge University Press

field is not periodic or steady. Indeed, in the latter case one cannot associate an extended dynamical system to $\mathbf{v}(\mathbf{x}, t)$ with a compact phase space given that t must be taken from all of $\mathbb{R}$.

2.2.14 Convergence of Time-Averaged Observables: Ergodic Theorems

Here we discuss how temporal averages of observed scalar fields relate to their spatial averages in perfectly mixing flows. We first state the results for averages taken under stroboscopic samplings (Poincaré maps) of the flow, then directly for the full flow. We first consider a Poincaré map $\mathbf{P}_{t_0} : S \to S$ defined on a physical domain S. As a special case of the general flow map $\mathbf{F}_{t_0}^t$, a Poincaré map of a smooth vector field is always a diffeomorphism (see §2.2.3). This will enable us to give a simplified treatment here relative to the more general results of *ergodic theory* (see, e.g., Walters, 1982).

Ergodic theory is concerned with the dynamics of maps on measurable subsets of S. The measures μ relevant for physically observable mixing in fluids are the volume when S is a 3D flow domain, the area (or the scaled areas, given by formulas (2.84) or (2.85)) when S is a 2D surface, and the arc length when S is a one-dimensional curve. Ergodic theory additionally requires S itself to have a finite measure $\mu(S)$. For practical applications to fluids, this finiteness assumption on μ amounts to the requirement that the domain S must be bounded.

We will assume that $\mathbf{P}_{t_0}$ is *measure preserving* on S, i.e., the measure of any subset $A \subset S$ is preserved under iterations of $\mathbf{P}_{t_0}$:

$$\mu(A) = \mu\left(\mathbf{P}_{t_0}^i(A)\right) \tag{2.86}$$

for all $i \geq 1$. This requirement holds for Poincaré maps of time-periodic incompressible flows and for extended Poincaré maps of time-quasiperiodic incompressible flows (see §2.2.12). As already noted, if the flow is compressible but conserves mass, then its associated stroboscopic maps are still measure preserving with respect to the fluid mass as a measure.

Note, however, that these conclusions about measure preservation only follow directly from the volume- or mass-preservation of the flow when S has the same dimension as the underlying velocity field $\mathbf{v}$. For instance, if $S \subset \mathbb{R}^2$ is an invariant curve in a 2D flow, then the 2D period-T map, $\mathbf{P}_{t_0}$, restricted to S is generally not a measure-preserving map on S. Examples of such invariant curves are stable or unstable manifolds of saddle-type fixed points, to be discussed later in §4.1.1. Along such invariant curves, $\mathbf{P}_{t_0}$ shrinks or expands the measure (arclength), respectively. Similarly, a measure-preserving Poincaré map, $\mathbf{P}_{t_0}$, on a 3D domain does not generally preserve any nondegenerate measure on a 2D invariant surface $\mathcal{M} = \mathbf{P}_{t_0}(\mathcal{M})$, as examples of 2D stable and unstable manifolds in 3D mappings illustrate. In contrast, Poincaré maps defined as first-return maps to a 2D transverse section S of 3D, steady, volume-preserving or mass-preserving flow are measure preserving on S with respect to the areas computed from the area elements (2.84) or (2.85).

We assume that the mapping $\mathbf{P}_{t_0}$ is *ergodic* on S, i.e., the invariant sets of $\mathbf{P}_{t_0}$ have either full measure or zero measure in S. This means that one cannot identify any experimentally observable part of S that does not mix with the rest of S under iterations of $\mathbf{P}_{t_0}$. For instance, the Poincaré map shown in Fig. 2.13(a) is *not* ergodic on the flow domain because the interiors of the two leapfrogging vortices are invariant subsets of nonzero area within the 2D Poincaré section S. The same map, however, *is* ergodic when restricted to its closed invariant

https://doi.org/10.1017/9781009225199.003 Published online by Cambridge University Press

curves because orbits within such elliptic transport barriers (see §4.1.2) are quasiperiodic and hence densely cover the barrier. As a consequence, there is no invariant set of nonzero arc length within the barrier. As another example, the Poincaré map shown in Fig. 2.13(b) is ergodic on its bounded 2D domain because the only invariant sets smaller than the full flow domain are the one-dimensional stable and unstable manifolds of its fixed points.

Consider now an *observable*, i.e., a scalar field $c(\mathbf{x})$ that is defined and integrable on the domain S of an ergodic, measure-preserving mapping $\mathbf{P}_{t_0}$.[14] Because of the perfect mixing of points in S under iterations of the ergodic map $\mathbf{P}_{t_0}$, one hopes to uncover dynamical features of $\mathbf{P}_{t_0}$ by averaging $c(\mathbf{x})$ along the orbits $\left\{\mathbf{x}_0, \mathbf{P}_{t_0}(\mathbf{x}_0), \mathbf{P}^2_{t_0}(\mathbf{x}_0), \ldots\right\}$ of $\mathbf{P}_{t_0}$. Indeed, *Birkhoff's ergodic theorem* (Birkhoff, 1931) guarantees that

$$\lim_{N\to\infty} \frac{1}{N} \sum_{k=1}^{N} c\left(\mathbf{P}^k_{t_0}(\mathbf{x}_0)\right) = \frac{1}{\mu(S)} \int_S c(\mathbf{x})\, d\mu$$

holds for *almost all* $\mathbf{x}_0 \in S$.[15] In other words, with the possible exception of an unobservable set of $\mathbf{x}_0$ locations, the temporal average of any observable along an orbit starting from $\mathbf{x}_0$ converges to the spatial average of that observable over the whole of S. For instance, if $c(\mathbf{x}) = x$ is the x-coordinate component of $\mathbf{x} = (x, y, z)$, then the averaged x-coordinate along a trajectory of a volume-preserving, ergodic Poincaré map, $\mathbf{P}_{t_0}(\mathbf{x}_0)$, is equal to $\frac{1}{\mu(S)} \int x\, d\mu$, the x-coordinate of the center of mass of the material set S.

In practice, velocity fields will generally not repeat themselves periodically in time and hence concepts from ergodic theory will not apply to them. Nevertheless, ergodicity is a useful conceptual tool for understanding and visualizing certain types of transport barriers (or lack thereof) in idealized model flows. Ergodicity also helps in interpreting mixing phenomena in low Reynolds number experiments whose velocity fields are very close to time-periodic (see Chapter 4).

A more general version of the classic ergodic theorem of Birkhoff is the *Birkhoff–Khinchin ergodic theorem*, which also applies to continuous flows of steady velocity fields (see Cornfeld et al., 1982). To state this theorem, we consider the flow map $\mathbf{F}^t : S \to S$ of a steady velocity field $\mathbf{v}(\mathbf{x})$ and a scalar field $c(\mathbf{x})$ whose integral exists with respect to a measure μ defined on the bounded and invariant 2D or 3D domain S. We assume that $\mathbf{F}^t$ preserves the measure μ, i.e., all subsets $\mathcal{A} \subset S$ satisfy $\mu(\mathbf{F}^t(\mathcal{A})) = \mu(\mathcal{A})$ for all times. For an incompressible flow, the measure μ preserved by $\mathbf{F}^t$ on the flow domain S is the volume or the area. For a mass-preserving flow on S, the measure preserved by $\mathbf{F}^t$ is the mass. If, however, S is a 2D invariant surface in a 3D flow, then $\mathbf{F}^t$ does not necessarily preserve any nondegenerate measure on S, even if it preserves volume or mass on the full 3D flow domain.

In analogy with the discrete case already discussed, we also assume that $\mathbf{F}^t$ is *ergodic on* S, i.e., the measure of any invariant sets of $\mathbf{F}^t$ in S is either zero or equal to $\mu(S)$. Then, according to the Birkhoff–Khinchin ergodic theorem (Cornfeld et al., 1982), for almost all initial conditions $\mathbf{x}_0 \in S$, we must have

[14] The observable c can also be a time-periodic scalar field, $c(\mathbf{x}, t) \equiv c(\mathbf{x}, t + T)$, where T is the time period of the underlying velocity field $\mathbf{v}(\mathbf{x}, t)$. The scalar field c does not even have to be smooth, but it has to be integrable with respect to the measure on S.

[15] Here "almost all" refers to all points $\mathbf{x}_0 \in S$ with the possible exception of a measure-zero subset of S.

https://doi.org/10.1017/9781009225199.003 Published online by Cambridge University Press

$$\lim_{t\to\infty}\frac{1}{t}\int_0^t c\left(\mathbf{F}^s(\mathbf{x}_0)\right)ds = \lim_{t\to\infty}\frac{1}{t}\int_0^t c\left(\mathbf{F}^{-s}(\mathbf{x}_0)\right)ds = \lim_{t\to\infty}\frac{1}{2t}\int_{-t}^t c\left(\mathbf{F}^s(\mathbf{x}_0)\right)ds$$
$$= \frac{1}{\mu(S)}\int_S c(\mathbf{x})\,d\mu. \tag{2.87}$$

In other words, with the possible exception of an unobservable set of $\mathbf{x}_0$ initial conditions, the forward, backward and full temporal averages of any observable along an orbit starting from $\mathbf{x}_0$ converge to the spatial average of the observable over the whole of S.

As we will see in examples in Chapter 4, typical 3D steady flows are not ergodic on their full domain D but might admit open ergodic subsets. More frequently, they admit 2D invariant surfaces (invariant tori) or 1D closed invariant curves (periodic orbits) restricted to which $\mathbf{F}^t$ becomes ergodic. Applying the Birkhoff–Khinchin ergodic theorem on the full domain D does not guarantee anything for averages of scalars taken over these lower-dimensional invariant surfaces given that those have measure zero in D. Thus, for all we know, these surfaces may be part of the set of locations that violate the Birkhoff–Khinchin ergodic theorem. The statement (2.87), therefore, is only meaningful for lower-dimensional invariant sets $S \subset D$ if the theorem is applicable directly to S with respect to a measure preserved by $\mathbf{F}^t$ on S. This measure is generally not known explicitly, but its existence is guaranteed by the type of dynamics (quasiperiodic or periodic) on these lower-dimensional invariant sets.

2.2.15 Lagrangian Scalars, Vector Fields and Tensors

We refer to scalar, vector and tensor fields defined over initial trajectory positions $\mathbf{x}_0$, initial times t_0 and current times t as *Lagrangian quantities*.

Specifically, we refer to scalar fields defined at arbitrary initial conditions $(\mathbf{x}_0, t_0)$ for all times t as *Lagrangian scalar* fields. For instance, a concentration field $c(\mathbf{x}, t)$ subject to advection and diffusion can be expressed as a Lagrangian scalar field $\hat{c}(\mathbf{x}_0, t_0; t) := c\left(\mathbf{F}_{t_0}^t(\mathbf{x}_0), t\right)$, depending on the current time t, initial time t_0 and the initial position $\mathbf{x}_0$ of the material trajectory that is at the point $\mathbf{x} = \mathbf{F}_{t_0}^t(\mathbf{x}_0)$ at time t.

A *Lagrangian vector field* is a time-dependent vector field $\mathbf{u}(\mathbf{x}_0, t_0; t)$ comprising vectors based in the tangent spaces $T_{\mathbf{x}_0}\mathbb{R}^n$ of $\mathbb{R}^n$ at the initial positions $\mathbf{x}_0 \in U$. These vectors remain based at the points $\mathbf{x}_0$ for all times $t \in [t_1, t_2]$ but they generally vary as functions of t. In contrast, an eigenvector field $\boldsymbol{\alpha}_i(\mathbf{x}_0; t_0, t)$ of a Lagrangian tensor field (to be defined below) is *not* a Lagrangian vector field because it has no well-defined length or orientation. Accordingly, we refer to such eigenvector fields as *Lagrangian direction fields*, in line with our terminology in §2.1.1 for the Eulerian case.

Despite their commonly used names, the *Lagrangian velocity* $\mathbf{v}\left(\mathbf{F}_{t_0}^t(\mathbf{x}_0), t\right)$ and the *Lagrangian vorticity* $\boldsymbol{\omega}\left(\mathbf{F}_{t_0}^t(\mathbf{x}_0), t\right)$ are *not* Lagrangian vector fields, as they comprise vectors based at the time-evolving current location $\mathbf{x}(t)$. In other words, these vector fields are pointwise elements of the tangent space $T_{\mathbf{F}_{t_0}^t(\mathbf{x}_0)}\mathbb{R}^n$, as opposed to $T_{\mathbf{x}_0}\mathbb{R}^n$,which would be required for a Lagrangian vector field.

In contrast, the *pullback velocity field* $\left[\mathbf{F}_{t_0}^t\right]^* \mathbf{v}$ and the *pullback vorticity field* $\left[\mathbf{F}_{t_0}^t\right]^* \boldsymbol{\omega}$, defined respectively as

https://doi.org/10.1017/9781009225199.003 Published online by Cambridge University Press

$$\left[\mathbf{F}_{t_0}^t\right]^* \mathbf{v}\left(\mathbf{x}_0, t_0; t\right) = \left[\nabla \mathbf{F}_{t_0}^t(\mathbf{x}_0)\right]^{-1} \mathbf{v}\left(\mathbf{F}_{t_0}^t(\mathbf{x}_0), t\right),$$
$$\left[\mathbf{F}_{t_0}^t\right]^* \boldsymbol{\omega}\left(\mathbf{x}_0, t_0; t\right) = \left[\nabla \mathbf{F}_{t_0}^t(\mathbf{x}_0)\right]^{-1} \boldsymbol{\omega}\left(\mathbf{F}_{t_0}^t(\mathbf{x}_0), t\right), \tag{2.88}$$

are Lagrangian vector fields, as both are elements of $T_{\mathbf{x}_0}\mathbb{R}^n$ for all values of t. In general, the pullback of a vector field with respect to a mapping is the most natural way to transport a vector field defined at current particle positions back to a vector field defined over initial positions, as shown in Fig. 2.17 for the velocity field. Similarly, the *pushforward velocity field*,

$$\left[\mathbf{F}_{t_0}^t\right]_* \mathbf{v}\left(\mathbf{x}, t; t_0\right) = \nabla \mathbf{F}_{t_0}^t(\mathbf{x}_0) \mathbf{v}\left(\mathbf{x}_0, t_0\right), \tag{2.89}$$

is a Lagrangian vector field with respect to the inverse flow map, comprising vectors defined in the tangent spaces $T_{\mathbf{x}}\mathbb{R}^n$ of current positions in $\mathbf{F}_{t_0}^t(U)$ (see Fig. 2.17).

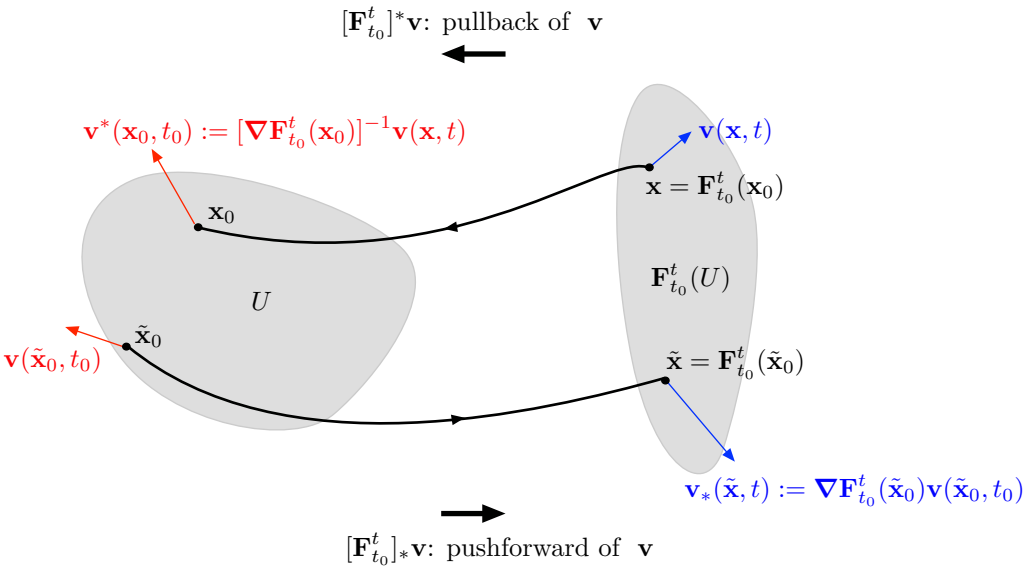

Figure 2.17 The geometry of the pullback $\mathbf{v}^* = \left[\mathbf{F}_{t_0}^t\right]^* \mathbf{v}$ and the pushforward $\mathbf{v}_* = \left[\mathbf{F}_{t_0}^t\right]_* \mathbf{v}$ of a velocity field $\mathbf{v}$ under the flow map $\mathbf{F}_{t_0}^t$.

A *Lagrangian tensor* $\mathbf{A}(\mathbf{x}_0, t_0; t)$ is a linear mapping of the tangent spaces $T_{\mathbf{x}_0}\mathbb{R}^n$ into themselves at all initial positions $\mathbf{x}_0$ for all times t. Despite its formal dependence on the same arguments, the deformation gradient $\nabla \mathbf{F}_{t_0}^t(\mathbf{x}_0)$ is not a Lagrangian tensor but a *two-point tensor* (see our discussion leading to formula (2.25) and Fig. 2.6), as it is a mapping between two different tangent spaces. In contrast, the *right Cauchy–Green strain tensor* (see §5.2.1),

$$\mathbf{C}_{t_0}^t(\mathbf{x}_0) = \left[\nabla \mathbf{F}_{t_0}^t(\mathbf{x}_0)\right]^{\mathrm{T}} \nabla \mathbf{F}_{t_0}^t(\mathbf{x}_0), \tag{2.90}$$

maps from the domain of $\nabla \mathbf{F}_{t_0}^t(\mathbf{x}_0)$ into the range of $\left[\nabla \mathbf{F}_{t_0}^t(\mathbf{x}_0)\right]^{\mathrm{T}}$. Therefore, by Eqs. (2.25) and (2.33), we can view this tensor pointwise as a linear operator

https://doi.org/10.1017/9781009225199.003 Published online by Cambridge University Press

$$\mathbf{C}_{t_0}^t(\mathbf{x}_0) : T_{\mathbf{x}_0}\mathbb{R}^n \to T_{\mathbf{x}_0}\mathbb{R}^n,$$

which renders $\mathbf{C}_{t_0}^t(\mathbf{x}_0)$ a Lagrangian tensor. By the same argument, the *left Cauchy–Green strain tensor* (see §5.2.1), defined as

$$\mathbf{B}_{t_0}^t(\mathbf{x}_0) = \nabla\mathbf{F}_{t_0}^t(\mathbf{x}_0)\left[\nabla\mathbf{F}_{t_0}^t(\mathbf{x}_0)\right]^{\mathrm{T}}, \tag{2.91}$$

maps from the domain of $\left[\nabla\mathbf{F}_{t_0}^t(\mathbf{x}_0)\right]^{\mathrm{T}}$ into the range of $\nabla\mathbf{F}_{t_0}^t(\mathbf{x}_0)$. Therefore, by Eqs. (2.25) and (2.33), we can view this tensor pointwise as a linear operator

$$\mathbf{B}_{t_0}^t(\mathbf{x}_0) : T_{\mathbf{F}_{t_0}^t(\mathbf{x}_0)}\mathbb{R}^n \to T_{\mathbf{F}_{t_0}^t(\mathbf{x}_0)}\mathbb{R}^n, \tag{2.92}$$

which renders $\mathbf{B}_{t_0}^t(\mathbf{x}_0)$ a Lagrangian tensor for the backward flow map $\left[\mathbf{F}_{t_0}^t(\mathbf{x}_0)\right]^{-1} = \mathbf{F}_t^{t_0}(\mathbf{x}_t)$. Alternatively, we can view

$$\mathbf{B}_{t_0}^t\left(\mathbf{F}_t^{t_0}(\mathbf{x})\right) : T_{\mathbf{x}}\mathbb{R}^n \to T_{\mathbf{x}}\mathbb{R}^n \tag{2.93}$$

as an Eulerian tensor (see §2.1.1). A direct calculation involving the definitions (2.90) and (2.91) of the right and left Cauchy–Green strain tensors, respectively, gives the relation

$$\left[\mathbf{C}_{t_0}^t\right]^{-1} = \left[\nabla\mathbf{F}_{t_0}^t\right]^{-1}\left[\nabla\mathbf{F}_{t_0}^t\right]^{-\mathrm{T}} = \nabla\mathbf{F}_t^{t_0}\left[\nabla\mathbf{F}_t^{t_0}\right]^{\mathrm{T}} = \mathbf{B}_t^{t_0}. \tag{2.94}$$

Let the eigenvalue problem associated with the symmetric, positive-definite tensor $\mathbf{C}_{t_0}^t(\mathbf{x}_0)$ be defined as

$$\mathbf{C}_{t_0}^t\boldsymbol{\xi}_i = \lambda_i\boldsymbol{\xi}_i, \tag{2.95}$$

with the eigenvalues

$$0 < \lambda_1(\mathbf{x}_0; t_0, t_1) \le \cdots \le \lambda_n(\mathbf{x}_0; t_0, t_1) \tag{2.96}$$

and orthonormal eigenvectors $\boldsymbol{\xi}_i(\mathbf{x}_0; t_0, t_1) \in T_{\mathbf{x}_0}\mathbb{R}^n$. We note that

$$\left|\nabla\mathbf{F}_{t_0}^t(\mathbf{x}_0)\boldsymbol{\xi}_i\right| = \sqrt{\left\langle\nabla\mathbf{F}_{t_0}^t(\mathbf{x}_0)\boldsymbol{\xi}_i, \nabla\mathbf{F}_{t_0}^t(\mathbf{x}_0)\boldsymbol{\xi}_i\right\rangle} = \sqrt{\left\langle\boldsymbol{\xi}_i, \mathbf{C}_{t_0}^t(\mathbf{x}_0)\boldsymbol{\xi}_i\right\rangle} = \sqrt{\lambda_i}, \tag{2.97}$$

and hence the deformation gradient stretches the eigenvectors of $\mathbf{C}_{t_0}^t(\mathbf{x}_0)$ by a factor equal to the square root of the corresponding eigenvalue.

Applying the operator $\nabla\mathbf{F}_{t_0}^t(\mathbf{x}_0)$ to both sides of the eigenvalue problem (2.95), using formula (2.97), then dividing both sides of the resulting equation by $\sqrt{\lambda_i}$ and defining the unit vectors $\boldsymbol{\eta}_i$ via the relation

$$\boldsymbol{\eta}_i(\mathbf{x}_0; t_0, t_1) = \frac{1}{\sqrt{\lambda_i}}\nabla\mathbf{F}_{t_0}^t(\mathbf{x}_0)\boldsymbol{\xi}_i(\mathbf{x}_0; t_0, t_1) \tag{2.98}$$

gives

$$\mathbf{B}_{t_0}^t\boldsymbol{\eta}_i = \lambda_i\boldsymbol{\eta}_i, \tag{2.99}$$

with the eigenvalues $0 < \lambda_1 \le \cdots \le \lambda_n$ coinciding with the eigenvalues of $\mathbf{C}_{t_0}^t$ introduced in formula (2.95). Therefore, Eq. (2.99) shows that the spectrum (i.e., the set of eigenvalues) of $\mathbf{B}_{t_0}^t$ coincides with the spectrum of $\mathbf{C}_{t_0}^t$. The corresponding unit eigenvectors $\boldsymbol{\eta}_i$ for $\mathbf{B}_{t_0}^t$ are given in Eq. (2.98).

In summary, the linearized flow maps the unit eigenvectors of the right Cauchy–Green strain tensor into the direction of the eigenvectors of the left Cauchy–Green strain tensor,

https://doi.org/10.1017/9781009225199.003 Published online by Cambridge University Press

scaled by the square root of the corresponding eigenvalue. Based on this observation, we sketch the geometry of the strain eigenvalues and eigenvectors in Fig. 2.18.

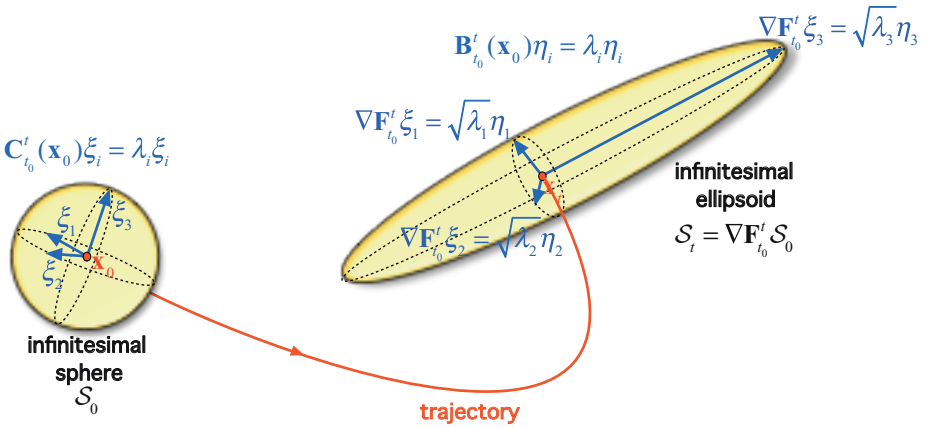

Figure 2.18 Deformation of a unit sphere based at $\mathbf{x}_0$ under the linearized flow map $\nabla\mathbf{F}^t_{t_0}(\mathbf{x}_0)$ into an ellipsoid along a trajectory $\mathbf{x}_t = \mathbf{F}^t_{t_0}(\mathbf{x}_0)$. The principal axes of the ellipsoid have lengths equal to the square roots of the eigenvalues λ_i of the right Cauchy–Green strain tensor $\mathbf{C}^t_{t_0}(\mathbf{x}_0)$. These axes are aligned with the unit eigenvectors $\boldsymbol{\eta}_i$ of the left Cauchy–Green strain tensor $\mathbf{B}^t_{t_0}(\mathbf{x}_0)$.

Switching the times t_0 and t in formula (2.94) and taking the inverse of both sides gives

$$\mathbf{C}^{t_0}_t = \left[\mathbf{B}^t_{t_0}\right]^{-1}. \tag{2.100}$$

Therefore, by formula (2.99), for the spectrum of the backward-time right Cauchy–Green tensor $\mathbf{C}^{t_0}_t$ we have

$$\text{spect}\left(\mathbf{C}^{t_0}_t\left(\mathbf{F}^t_{t_0}(\mathbf{x}_0)\right)\right) = \text{spect}\left(\left[\mathbf{C}^t_{t_0}(\mathbf{x}_0)\right]^{-1}\right) = \left\{\frac{1}{\lambda_1(\mathbf{x}_0;t_0,t_1)},\ldots,\frac{1}{\lambda_n(\mathbf{x}_0;t_0,t_1)}\right\}, \tag{2.101}$$

even though $\mathbf{C}^{t_0}_t \neq \left[\mathbf{C}^t_{t_0}\right]^{-1}$, as pointed out in Haller and Sapsis (2011). Furthermore, by Eq. (2.100), the unit eigenvectors of $\mathbf{C}^{t_0}_t$ coincide with those of $\mathbf{B}^t_{t_0}$ and hence we have

$$\mathbf{C}^{t_0}_t\boldsymbol{\eta}_i = \frac{1}{\lambda_i}\boldsymbol{\eta}_i, \quad \boldsymbol{\eta}_i(\mathbf{x}_0;t_0,t) = \boldsymbol{\xi}_i(\mathbf{x}_0;t_0,t), \quad i = 1,2,3. \tag{2.102}$$

In two dimensions, if both pairs $(\boldsymbol{\xi}_1,\boldsymbol{\xi}_2)$ and $(\boldsymbol{\eta}_1,\boldsymbol{\eta}_2)$ are selected to have the same orientation, then we can define an orthogonal rotation tensor $\mathbf{R}_{\pi/2}$ so that

$$\boldsymbol{\xi}_2 = \mathbf{R}_{\pi/2}\boldsymbol{\xi}_1, \qquad \boldsymbol{\eta}_2 = \mathbf{R}_{\pi/2}\boldsymbol{\eta}_1. \tag{2.103}$$

In §2.3.2, we will also identify the linear operator, represented by the polar rotation tensor $\mathbf{R}^t_{t_0}$, that rotates all unit eigenvectors $\boldsymbol{\xi}_i$ into the unit eigenvectors $\boldsymbol{\eta}_i$ in any dimension. For 2D flows, using the tensor $\mathbf{R}^t_{t_0}$ and the relations (2.103), we therefore obtain

$$\begin{aligned}\langle\boldsymbol{\xi}_1,\boldsymbol{\eta}_1\rangle &= \left\langle\boldsymbol{\xi}_1,\mathbf{R}^t_{t_0}\boldsymbol{\xi}_1\right\rangle = \left\langle\mathbf{R}^{-1}_{\pi/2}\boldsymbol{\xi}_2,\mathbf{R}^t_{t_0}\mathbf{R}^{-1}_{\pi/2}\boldsymbol{\xi}_2\right\rangle = \left\langle\boldsymbol{\xi}_2,\mathbf{R}^t_{t_0}\mathbf{R}^1_{\pi/2}\mathbf{R}^{-1}_{\pi/2}\boldsymbol{\xi}_2\right\rangle = \left\langle\boldsymbol{\xi}_2,\mathbf{R}^t_{t_0}\boldsymbol{\xi}_2\right\rangle \\ &= \langle\boldsymbol{\xi}_2,\boldsymbol{\eta}_2\rangle,\end{aligned} \tag{2.104}$$

https://doi.org/10.1017/9781009225199.003 Published online by Cambridge University Press

because all rotations commute in two dimensions.

We also mention a further Lagrangian strain tensor that has been used in continuum mechanics. This tensor, the *Green–Lagrange strain tensor*, is defined as

$$\mathbf{E}_{t_0}^{t} = \frac{1}{2}\left[\mathbf{C}_{t_0}^{t} - \mathbf{I}\right], \tag{2.105}$$

and measures how close the material deformation is to the identity mapping. Note that the eigenvectors of this tensor coincide with the eigenvectors of $\mathbf{C}_{t_0}^{t}$ with corresponding eigenvalues $\lambda_i(\mathbf{x}_0; t_0, t) - 1$ for $i = 1, \ldots, n$.

We close by noting a property for 2D ($n = 2$) symmetric, nonsingular Lagrangian tensors $\mathbf{A}(\mathbf{x}_0, t_0; t) = \mathbf{A}^{\mathrm{T}}(\mathbf{x}_0, t_0; t)$, such as the strain tensors $\mathbf{C}_{t_0}^{t}$ and $\mathbf{B}_{t_0}^{t}$ for 2D flows. For any such tensor, one can verify in coordinates the identity

$$\mathbf{J}^{\mathrm{T}}\mathbf{A}\mathbf{J} = (\det \mathbf{A})\,\mathbf{A}^{-1}, \qquad \mathbf{J} = \begin{pmatrix} 0 & 1 \\ -1 & 0 \end{pmatrix}, \tag{2.106}$$

which we will use repeatedly in later chapters.

2.3 Lagrangian Decompositions of Infinitesimal Material Deformation

Various approaches exist for identifying qualitatively different components of the deformation of material elements along trajectories. These decompositions have proven useful in isolating material properties of perceived purely advective transport barriers (or coherent structures). For later use, we survey here three available decompositions of the deformation gradient: the singular value decomposition (SVD), the polar decomposition (PD) and the dynamic polar decomposition (DPD). While these decompositions into rotation and deformation apply to more general linear operators as well, we will only discuss them here for the deformation gradient.

2.3.1 Singular Value Decomposition (SVD)

By a fundamental result in linear algebra, the nonsingular linear operator $\nabla\mathbf{F}_{t_0}^{t}(\mathbf{x}_0)$ can be decomposed into a product

$$\nabla\mathbf{F}_{t_0}^{t} = \mathbf{P}_{t_0}^{t}\,\mathbf{\Sigma}_{t_0}^{t}\left[\mathbf{Q}_{t_0}^{t}\right]^{\mathrm{T}}, \tag{2.107}$$

where $\mathbf{P}_{t_0}^{t}$ and $\mathbf{Q}_{t_0}^{t}$ are proper orthogonal matrices and $\mathbf{\Sigma}_{t_0}^{t}$ is a positive-definite diagonal matrix (Golub and Van Loan, 2013). Therefore, $\mathbf{P}_{t_0}^{t}$ and $\mathbf{Q}_{t_0}^{t}$ represent rotations and $\mathbf{\Sigma}_{t_0}^{t}$ represents the combination of n independent, uniaxial compressions or extensions in mutually orthogonal directions.

Specifically, in terms of the strain eigenvalues λ_i and unit eigenvectors $\boldsymbol{\xi}_i$ and $\boldsymbol{\eta}_i$ defined in the Cauchy–Green strain eigenvalue problems (2.95) and (2.99), we have

$$\mathbf{\Sigma}_{t_0}^{t} = \begin{pmatrix} \sqrt{\lambda_1} & \cdots & 0 \\ \vdots & \ddots & \vdots \\ 0 & \cdots & \sqrt{\lambda_n} \end{pmatrix}, \quad \mathbf{P}_{t_0}^{t} = [\boldsymbol{\eta}_i, \ldots, \boldsymbol{\eta}_n], \quad \mathbf{Q}_{t_0}^{t} = [\boldsymbol{\xi}_i, \ldots, \boldsymbol{\xi}_n]. \tag{2.108}$$

https://doi.org/10.1017/9781009225199.003 Published online by Cambridge University Press

In this context, the $\boldsymbol{\eta}_i$ are called the *left singular vectors* and the $\boldsymbol{\xi}_i$ the *right singular vectors* of the deformation gradient $\boldsymbol{\nabla}\mathbf{F}_{t_0}^t$. The diagonal entries $\sqrt{\lambda_i}$ are called the corresponding *singular values of* $\boldsymbol{\nabla}\mathbf{F}_{t_0}^t$. Apart from the ordering of singular values and singular vectors, the decomposition (2.107) is unique. The geometry of the two rotations, $\left[\mathbf{Q}_{t_0}^t\right]^{\mathrm{T}}$ and $\mathbf{P}_{t_0}^t$, together with that of the stretching-compression $\boldsymbol{\Sigma}_{t_0}^t$, is shown in Fig. 2.19. The figure also illustrates that

$$\boldsymbol{\Sigma}_{t_0}^t : T_{\mathbf{x}_0}\mathbb{R}^n \to T_{\mathbf{x}}\mathbb{R}^n \tag{2.109}$$

is a two-point tensor (see §2.2.15), just like the deformation gradient $\boldsymbol{\nabla}\mathbf{F}_{t_0}^t$.

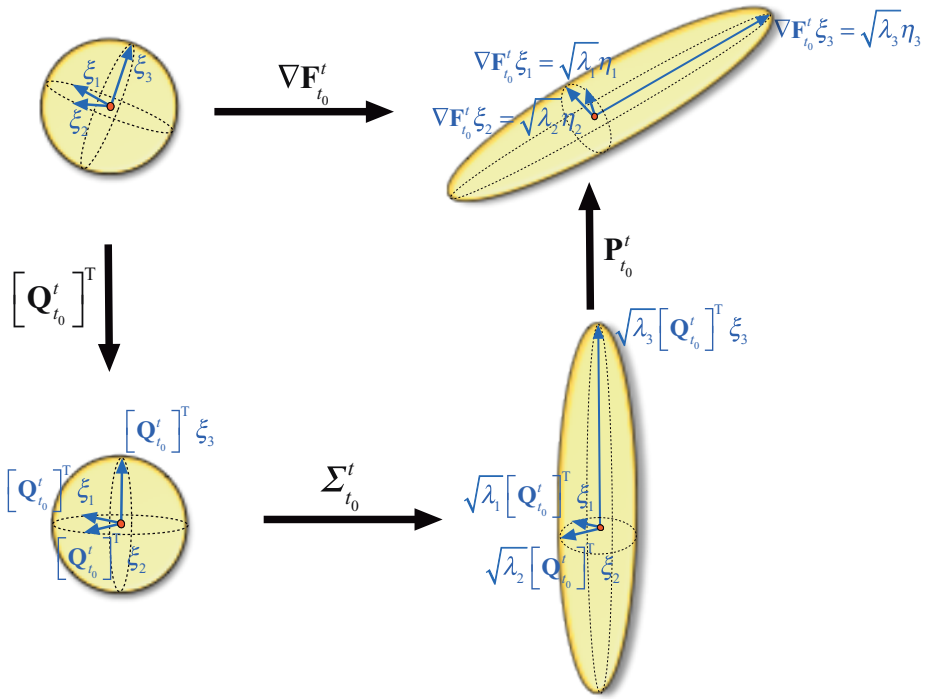

Figure 2.19 The geometric meaning of the rotation tensors $\mathbf{Q}_{t_0}^t$ and $\mathbf{P}_{t_0}^t$, together with the triaxial stretching-compression tensor $\boldsymbol{\Sigma}_{t_0}^t$ involved in the singular value decomposition (2.107) of the deformation gradient $\boldsymbol{\nabla}\mathbf{F}_{t_0}^t$.

A classic use of SVD is for the solution of linear algebraic equations. In our context, SVD is a quick and accurate tool for identifying the eigenvectors of the right and left Cauchy–Green strain tensors, which arise in several coherent structure detection methods discussed in later chapters.

The computation of the SVD of the deformation gradient for 2D and 3D flows is implemented in Notebooks 2.3 and 2.4, respectively.

https://doi.org/10.1017/9781009225199.003 Published online by Cambridge University Press

Notebook 2.3 (SVD2D) *Computes the singular value decomposition (SVD) of the deformation gradient* $\nabla \mathbf{F}_{t_0}^t$ *for a 2D velocity data set.*
https://github.com/haller-group/TBarrier/tree/main/TBarrier/2D/demos/Decompositions/SVD2D

Notebook 2.4 (SVD3D) *Computes the singular value decomposition (SVD) of the deformation gradient* $\nabla \mathbf{F}_{t_0}^t$ *for a 3D velocity data set.*
https://github.com/haller-group/TBarrier/tree/main/TBarrier/3D/demos/Decompositions/SVD3D

2.3.2 Polar Decomposition

By the *polar decomposition theorem*, at any initial location $\mathbf{x}_0$, the deformation gradient $\nabla \mathbf{F}_{t_0}^t(\mathbf{x}_0)$ can also be uniquely decomposed as

$$\nabla \mathbf{F}_{t_0}^t = \mathbf{R}_{t_0}^t \mathbf{U}_{t_0}^t = \mathbf{V}_{t_0}^t \mathbf{R}_{t_0}^t, \tag{2.110}$$

with the proper orthogonal *rotation tensor* $\mathbf{R}_{t_0}^t$, the symmetric and positive definite *right stretch tensor* $\mathbf{U}_{t_0}^t$ and the symmetric and positive definite *left stretch tensor* $\mathbf{V}_{t_0}^t$ (Gurtin et al., 2010; Truesdell, 1992). One can verify by direct substitution into Eq. (2.110) that these tensors must be of the form

$$\mathbf{U}_{t_0}^t = \left[\mathbf{C}_{t_0}^t\right]^{1/2}, \qquad \mathbf{V}_{t_0}^t = \left[\mathbf{B}_{t_0}^t\right]^{1/2}, \qquad \mathbf{R}_{t_0}^t = \nabla \mathbf{F}_{t_0}^t \left[\mathbf{U}_{t_0}^t\right]^{-1} = \left[\mathbf{V}_{t_0}^t\right]^{-1} \nabla \mathbf{F}_{t_0}^t, \tag{2.111}$$

with $\mathbf{C}_{t_0}^t$ and $\mathbf{B}_{t_0}^t$ denoting the right and left Cauchy–Green strain tensors, respectively, as defined in Eqs. (2.90) and (2.91). The decomposition (2.110) means that a general deformation can locally always be viewed as triaxial stretching and compression followed by a rigid-body rotation, or as a rigid-body rotation followed by triaxial stretching and compression, as shown in Fig. 2.20. The figure also illustrates that

$$\mathbf{R}_{t_0}^t : T_{\mathbf{x}_0}\mathbb{R}^n \to T_{\mathbf{x}}\mathbb{R}^n \tag{2.112}$$

is a two-point tensor (see §3.50), whereas

$$\begin{aligned} \mathbf{U}_{t_0}^t &: T_{\mathbf{x}_0}\mathbb{R}^n \to T_{\mathbf{x}_0}\mathbb{R}^n, \\ \mathbf{V}_{t_0}^t &: T_{\mathbf{x}}\mathbb{R}^n \to T_{\mathbf{x}}\mathbb{R}^n \end{aligned} \tag{2.113}$$

are Lagrangian and Eulerian tensors, respectively (see §§2.2.15 and 2.1.1).

The polar rotation tensor $\mathbf{R}_{t_0}^t$ also turns out to be the closest rotation tensor to $\nabla \mathbf{F}_{t_0}^t$ in the Frobenius matrix norm (see Neff et al., 2014). A further geometrically appealing property of the polar rotation is obtained by applying the deformation gradient to the Cauchy–Green eigenvector $\boldsymbol{\xi}_i$ and using the relations (2.110)–(2.111), which yields

$$\nabla \mathbf{F}_{t_0}^t \boldsymbol{\xi}_i = \mathbf{R}_{t_0}^t \mathbf{U}_{t_0}^t \boldsymbol{\xi}_i = \mathbf{R}_{t_0}^t \left[\mathbf{C}_{t_0}^t\right]^{1/2} \boldsymbol{\xi}_i = \sqrt{\lambda_i} \mathbf{R}_{t_0}^t \boldsymbol{\xi}_i.$$

Comparing this formula with Eq. (2.98) then gives the result

$$\mathbf{R}_{t_0}^t \boldsymbol{\xi}_i = \boldsymbol{\eta}_i, \tag{2.114}$$

https://doi.org/10.1017/9781009225199.003 Published online by Cambridge University Press

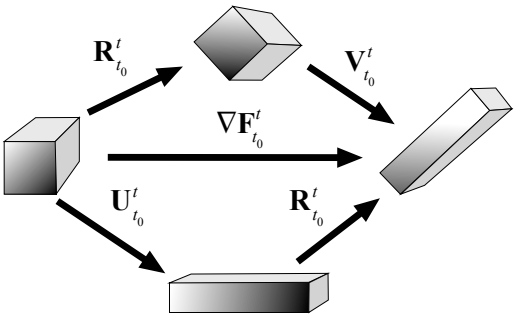

Figure 2.20 The geometric meaning of the polar rotation tensor, the left stretch tensor and the right stretch tensor, with their actions illustrated on an infinitesimal material cube.

showing that the polar rotation rotates the eigenvectors of $\mathbf{C}^t_{t_0}$ into those of $\mathbf{B}^t_{t_0}$. Substituting the polar decomposition formula (2.110) into the definitions (2.95) and (2.99) of the right and left Cauchy–Green strain tensors, respectively, we obtain

$$\mathbf{C}^t_{t_0} = \mathbf{U}^t_{t_0}\mathbf{U}^t_{t_0} = \left[\mathbf{U}^t_{t_0}\right]^{\mathrm{T}}\mathbf{U}^t_{t_0}, \qquad \mathbf{B}^t_{t_0} = \mathbf{V}^t_{t_0}\mathbf{V}^t_{t_0} = \left[\mathbf{V}^t_{t_0}\right]^{\mathrm{T}}\mathbf{V}^t_{t_0}.$$

This shows that the singular values and singular vectors of $\mathbf{U}^t_{t_0}$ coincide with the eigenvalues and eigenvectors of $\mathbf{C}^t_{t_0}$; a similar relationship holds between $\mathbf{V}^t_{t_0}$ and $\mathbf{B}^t_{t_0}$.

The computation of the polar decomposition of the deformation gradient for 2D and 3D flows is implemented in Notebooks 2.5 and 2.6, respectively.

Notebook 2.5 (PD2D) *Computes the polar decomposition (PD) of the deformation gradient* $\nabla\mathbf{F}^t_{t_0}$ *for a 2D velocity data set.*
https://github.com/haller-group/TBarrier/tree/main/TBarrier/2D/demos/Decompositions/PD2D

Notebook 2.6 (PD3D) *Computes the polar decomposition (PD) of the deformation gradient* $\nabla\mathbf{F}^t_{t_0}$ *for a 3D velocity data set.*
https://github.com/haller-group/TBarrier/tree/main/TBarrier/3D/demos/Decompositions/PD3D

To associate a rotation angle with polar rotations, we recall the Rodrigues formula (see Basar and Weichert, 2000) by which $\mathbf{R}^t_{t_0}$, as any 3D rotation, can be written in the form

$$\mathbf{R}^t_{t_0} = \mathbf{I} + \sin\Theta\mathbf{P} + (1-\cos\Theta)\,\mathbf{P}^2, \qquad \mathbf{P} = \begin{pmatrix} 0 & -k_3 & k_2 \\ k_3 & 0 & -k_1 \\ -k_2 & k_1 & 0 \end{pmatrix}, \quad |\mathbf{k}| = 1. \tag{2.115}$$

Here, the skew-symmetric matrix $\mathbf{P}$ is determined by the unit vector $\mathbf{k} = (k_1, k_2, k_3)$ defining the axis of the rotation performed by $\mathbf{R}^t_{t_0}$, and the *polar rotation angle* (PRA),

$$\mathrm{PRA}^t_{t_0}(\mathbf{x}_0) := \Theta(\mathbf{x}_0), \tag{2.116}$$

https://doi.org/10.1017/9781009225199.003 Published online by Cambridge University Press

is the angle of rotation generated by $\mathbf{R}_{t_0}^t$ around $\mathbf{k}$.

By formula (2.112), $\mathbf{R}_{t_0}^t$ is a two-point tensor and hence its trace is no longer an invariant (see §3.5).[16] Keeping that in mind, we take the trace of both sides of the equation in (2.115), Farazmand and Haller (2016) obtain that the polar rotation angle satisfies

$$\cos\left[\mathrm{PRA}_{t_0}^t(\mathbf{x}_0)\right] = \frac{1}{2}\left(\mathrm{tr}\,\mathbf{R}_{t_0}^t(\mathbf{x}_0) - 1\right). \tag{2.117}$$

Here, we have pointed out the dependence of this rotation angle on the initial position $\mathbf{x}_0$, as well as on the initial time t_0 and the current time t.

Choosing $\{\boldsymbol{\xi}_i\}_{i=1}^3$ (i.e., the eigenbasis of the right Cauchy–Green strain tensor $\mathbf{C}_{t_0}^t(\mathbf{x}_0)$) as a basis in $T_{\mathbf{x}_0}\mathbb{R}^n$ and parallel-translating this basis to obtain another basis in $T_{\mathbf{x}}\mathbb{R}^n$, we can specifically compute $\mathrm{tr}\,\mathbf{R}_{t_0}^t$ in this set of bases and use formula (2.114) to obtain

$$\mathrm{tr}\,\mathbf{R}_{t_0}^t = \sum_{i=1}^3 \left\langle \boldsymbol{\xi}_i, \mathbf{R}_{t_0}^t \boldsymbol{\xi}_i \right\rangle = \sum_{i=1}^3 \langle \boldsymbol{\xi}_i, \boldsymbol{\eta}_i \rangle, \tag{2.118}$$

with the inner product computed by parallel-translating $\boldsymbol{\xi}_i$ into $T_{\mathbf{x}}\mathbb{R}^n$.[17] Thus, as noted by Kulkarni (2021), Eqs. (2.117)–(2.118) imply that in the chosen set of bases, the PRA can be computed from the strain eigenvectors as

$$\mathrm{PRA}_{t_0}^t(\mathbf{x}_0) = \cos^{-1}\left[\frac{1}{2}\left(\sum_{i=1}^3 \langle \boldsymbol{\xi}_i, \boldsymbol{\eta}_i \rangle - 1\right)\right], \tag{2.119}$$

with $\boldsymbol{\xi}_i$ and $\boldsymbol{\eta}_i$ computed as right and left singular vectors of $\boldsymbol{\nabla}\mathbf{F}_{t_0}^t(\mathbf{x}_0)$, as in Eq. (2.108).

For 2D flows, setting $k_3 = 1$ and $k_1 = k_2 = 0$, then taking the trace of both sides of Eq. (2.115) and using formula (2.104) gives

$$\begin{aligned}\cos \mathrm{PRA}_{t_0}^t(\mathbf{x}_0) &= \frac{1}{2}\mathrm{tr}\,\mathbf{R}_{t_0}^t(\mathbf{x}_0) = \frac{1}{2}\sum_{i=1}^2 \left\langle \boldsymbol{\xi}_i, \mathbf{R}_{t_0}^t \boldsymbol{\xi}_i \right\rangle \\ &= \langle \boldsymbol{\xi}_1, \boldsymbol{\eta}_1 \rangle = \langle \boldsymbol{\xi}_2, \boldsymbol{\eta}_2 \rangle,\end{aligned} \tag{2.120}$$

yielding the 2D analogue of the polar rotation angle formula (2.119) in the form

$$\mathrm{PRA}_{t_0}^t(\mathbf{x}_0) = \cos^{-1}\langle \boldsymbol{\xi}_1, \boldsymbol{\eta}_1 \rangle = \cos^{-1}\langle \boldsymbol{\xi}_2, \boldsymbol{\eta}_2 \rangle, \tag{2.121}$$

as noted by Kulkarni (2021).

The polar decomposition is an appealing tool in continuum mechanics for decomposing linearized material deformation between fixed initial and final configurations. This decomposition, however, also has a lesser known disadvantage under variations of the initial and final configurations. Namely, polar rotation tensors computed over adjacent time intervals cannot be superimposed, i.e., they do not form a self-consistent family of subsequent rigid-body rotations. Specifically, for any two adjacent time intervals $[\tau, s]$ and $[s, t]$, we generally have

$$\mathbf{R}_\tau^t \neq \mathbf{R}_s^t \mathbf{R}_\tau^s, \tag{2.122}$$

[16] The Rodrigues formula is for rotation matrices mapping a linear space into itself, and hence the formula (2.115) is only valid if the basis used in $T_{\mathbf{x}_0}\mathbb{R}^n$ is parallel-translated to $T_{\mathbf{F}_{t_0}^t(\mathbf{x}_0)}\mathbb{R}^n$. This implies that the Rodrigues formula and the $\mathrm{PRA}_{t_0}^t(\mathbf{x}_0)$ depend on the frames of reference chosen in $T_{\mathbf{x}_0}\mathbb{R}^n$ and $T_{\mathbf{F}_{t_0}^t(\mathbf{x}_0)}\mathbb{R}^n$.

[17] In other words, the inner product can be evaluated as if $\boldsymbol{\xi}_i$ and $\boldsymbol{\eta}_i$ were elements of the same linear space.

https://doi.org/10.1017/9781009225199.003 Published online by Cambridge University Press

as illustrated in Fig. 2.21 (see Haller, 2016). This *dynamical inconsistency* implies, for instance, that $\mathbf{R}_\tau^t$ cannot be obtained from a sequence of incremental computations starting from time τ.

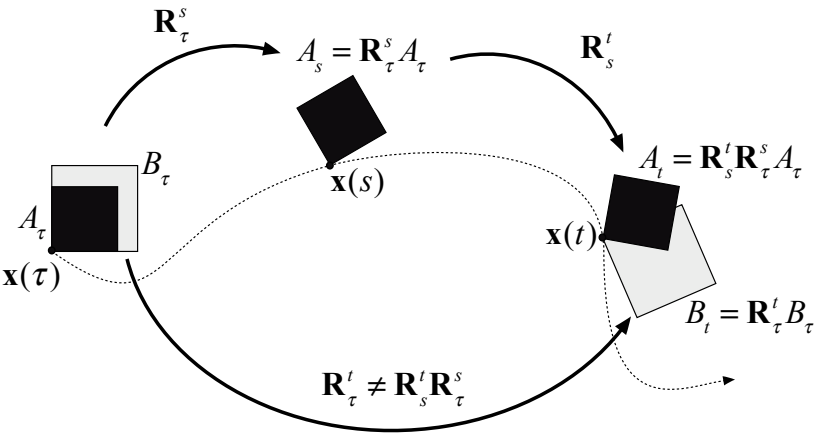

Figure 2.21 Dynamical inconsistency of polar rotations. The action of the polar rotations $\mathbf{R}_\tau^t$, $\mathbf{R}_\tau^s$ and $\mathbf{R}_s^t$, illustrated on two infinitesimal, geometric volume elements A_τ and B_τ, based at the same initial point at time τ. The evolution of A_τ is shown incrementally under the subsequent rotations $\mathbf{R}_\tau^s$ and $\mathbf{R}_s^t$. The evolution of the volume B_τ (with initial orientation identical to that of A_τ) is shown under the polar rotation $\mathbf{R}_\tau^t$. All volume elements shown are nonmaterial: they only serve to illustrate how orthogonal directions are rotated by the various polar rotations involved.

The dynamical inconsistency of $\mathbf{R}_\tau^t$ does not imply any flaw in the mathematics of the polar decomposition, yet creates a need for another decomposition that can identify a truly materially evolving (and hence dynamically consistent) rotation component for the time-evolving deformation gradient $\nabla \mathbf{F}_{t_0}^t$. Next, we describe such a decomposition.

2.3.3 Dynamic Polar Decomposition (DPD)

To address the dynamic inconsistency (2.122) of the classic polar rotation, Haller (2016) derives a dynamic version of this decomposition for time-dependent families of linear operators. We spell out this general result here specifically for the deformation gradient. For the statement of the main result, we will use the spin tensor $\mathbf{W}$ and the rate-of-strain tensor $\mathbf{S}$ defined in Eq. (2.1). The spatial mean of the spin tensor over the entire evolving fluid mass of interest, $D(t) = \mathbf{F}_{t_0}^t\,(D(t_0))$, will be denoted by the *mean-spin tensor*

$$\bar{\mathbf{W}}(t) = \frac{1}{\operatorname{vol} D(t)} \int_{D(t)} \mathbf{W}(\mathbf{x}, t)\, dV. \tag{2.123}$$

https://doi.org/10.1017/9781009225199.003 Published online by Cambridge University Press

As shown by Haller (2016), the deformation gradient $\nabla \mathbf{F}_{t_0}^t(\mathbf{x}_0)$ admits a unique decomposition of the form

$$\nabla \mathbf{F}_{t_0}^t = \mathbf{O}_{t_0}^t \mathbf{M}_{t_0}^t = \mathbf{N}_{t_0}^t \mathbf{O}_{t_0}^t, \tag{2.124}$$

where the proper orthogonal *dynamic rotation tensor,* $\mathbf{O}_{t_0}^t$, is the deformation gradient of a purely rotational flow, and the *right dynamic stretch tensor* $\mathbf{M}_{t_0}^t$ and the transpose of the non-degenerate *left dynamic stretch tensor* $\mathbf{N}_{t_0}^t$ are deformation gradients of purely straining flows. Specifically, these tensors satisfy the initial-value problems

$$\dot{\mathbf{O}}_{t_0}^t = \mathbf{W}\left(\mathbf{F}_{t_0}^t(\mathbf{x}_0), t\right) \mathbf{O}_{t_0}^t, \qquad \mathbf{O}_{t_0}^{t_0} = \mathbf{I}, \tag{2.125}$$

$$\dot{\mathbf{M}}_{t_0}^t = \left[\mathbf{O}_t^{t_0} \mathbf{S}\left(\mathbf{F}_{t_0}^t(\mathbf{x}_0), t\right) \mathbf{O}_{t_0}^t\right] \mathbf{M}_{t_0}^t, \qquad \mathbf{M}_{t_0}^{t_0} = \mathbf{I}, \tag{2.126}$$

$$\frac{d}{dt_0}\left(\mathbf{N}_{t_0}^t\right)^{\mathrm{T}} = -\left[\mathbf{O}_{t_0}^t \mathbf{S}\left(\mathbf{F}_t^{t_0}(\mathbf{x}_t), t_0\right) \mathbf{O}_t^{t_0}\right]\left(\mathbf{N}_{t_0}^t\right)^{\mathrm{T}}, \qquad \left(\mathbf{N}_t^t\right)^{\mathrm{T}} = \mathbf{I}. \tag{2.127}$$

The geometric meaning of the dynamic tensors $\mathbf{O}_{t_0}^t$, $\mathbf{M}_{t_0}^t$ and $\mathbf{N}_{t_0}^t$ is similar to that of $\mathbf{R}_{t_0}^t, \mathbf{U}_{t_0}^t$ and $\mathbf{V}_{t_0}^t$ shown in Fig. 2.20. Correspondingly, $\mathbf{O}_{t_0}^t$ is also a two-point tensor, while $\mathbf{M}_{t_0}^t$ and $\mathbf{N}_{t_0}^t$ are Lagrangian and Eulerian tensors, respectively. However, the dynamic rotation tensor $\mathbf{O}_{t_0}^t$, as the fundamental matrix solution of a linear ordinary differential equation (see Arnold, 1978), satisfies the group property

$$\mathbf{O}_{t_0}^t = \mathbf{O}_s^t \mathbf{O}_{t_0}^s, \qquad s, t \in [t_0, t_1], \tag{2.128}$$

and hence is dynamically consistent. The tensor $\mathbf{O}_{t_0}^t$ represents twice the mean material rotation observed for any small, passive rigid object (vorticity meter) carried on the surface of fluid flows in experiments (see Shapiro, 1961; Haller, 2016). This tensor also admits a further factorization

$$\mathbf{O}_{t_0}^t = \mathbf{\Phi}_{t_0}^t \mathbf{\Theta}_{t_0}^t, \tag{2.129}$$

into the *relative rotation tensor* $\mathbf{\Phi}_{t_0}^t$ and the *mean rotation tensor* $\mathbf{\Theta}_{t_0}^t$, which satisfy the initial value problems

$$\begin{aligned} \dot{\mathbf{\Phi}}_{t_0}^t &= \left[\mathbf{W}\left(\mathbf{F}_{t_0}^t(\mathbf{x}_0), t\right) - \bar{\mathbf{W}}(t)\right] \mathbf{\Phi}_{t_0}^t, & \mathbf{\Phi}_{t_0}^{t_0} &= \mathbf{I}, \\ \dot{\mathbf{\Theta}}_{t_0}^t &= \left[\mathbf{\Phi}_t^{t_0} \bar{\mathbf{W}}(t) \mathbf{\Phi}_{t_0}^t\right] \mathbf{\Theta}_{t_0}^t, & \mathbf{\Theta}_{t_0}^{t_0} &= \mathbf{I}, \end{aligned} \tag{2.130}$$

with the mean-spin tensor $\bar{\mathbf{W}}(t)$ defined in Eq. (2.123). The relative rotation tensor, $\mathbf{\Phi}_{t_0}^t$, as the fundamental solution matrix of a linear ordinary differential equation, is also dynamically consistent. The mean rotation tensor, $\mathbf{\Theta}_{t_0}^t$, however, solves a differential equation with memory, just as $\mathbf{M}_{t_0}^t$ and $\mathbf{N}_{t_0}^t$ do. Indeed, the coefficient matrices of these linear differential equations depend explicitly on the initial time t_0. As a consequence, $\mathbf{\Theta}_{t_0}^t$, $\mathbf{M}_{t_0}^t$ and $\mathbf{N}_{t_0}^t$ are not dynamically consistent.

The computation of the dynamic polar decomposition of the deformation gradient for 2D and 3D flows is implemented in Notebooks 2.7 and 2.8, respectively.

Notebook 2.7 (DPD2D) *Computes the dynamic polar decomposition (DPD) of the deformation gradient* $\nabla \mathbf{F}_{t_0}^t$ *for a 2D velocity data set.*
https://github.com/haller-group/TBarrier/tree/main/TBarrier/2D/demos/Decompositions/DPD2D

https://doi.org/10.1017/9781009225199.003 Published online by Cambridge University Press

Notebook 2.8 (DPD3D) *Computes the dynamic polar decomposition (DPD) of the deformation gradient* $\nabla \mathbf{F}_{t_0}^t$ *for a 3D velocity data set.*
https://github.com/haller-group/TBarrier/tree/main/TBarrier/3D/demos/Decompositions/DPD3D

Haller (2016) shows that the instantaneous axis of rotation associated with the relative rotation tensor $\mathbf{\Phi}_{t_0}^t$ is aligned with the vector $-\left[\boldsymbol{\omega}\left(\mathbf{F}_{t_0}^t(\mathbf{x}_0), t\right) - \bar{\omega}(t)\right]$, where

$$\bar{\omega}(t) = \frac{1}{\operatorname{vol} D(t)} \int_{D(t)} \boldsymbol{\omega}(\mathbf{x}, t)\, dV \tag{2.131}$$

is the mean vorticity of the fluid mass $D(t)$. The total accumulated rotation (total angle swept with no regard to direction) experienced by any vector under the action of $\mathbf{\Phi}_{t_0}^t$ around this time-varying rotation axis is given by the *intrinsic dynamic rotation angle*

$$\psi_{t_0}^t(\mathbf{x}_0) = \frac{1}{2} \int_{t_0}^{t} \left|\boldsymbol{\omega}(\mathbf{F}_{t_0}^s(\mathbf{x}_0), s) - \bar{\omega}(s)\right| ds, \tag{2.132}$$

as illustrated in Fig. 2.22.

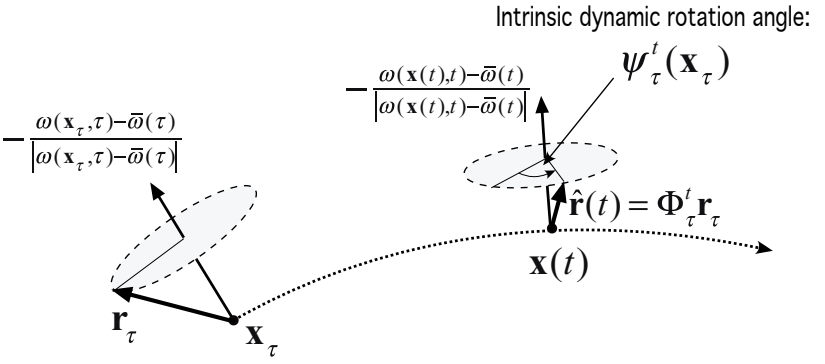

Figure 2.22 The geometry of the intrinsic dynamic rotation angle as the total angle swept by an arbitrary initial vector $\mathbf{r}_\tau$ (based at an initial location $\mathbf{x}_\tau$ at time τ) under the action of the relative rotation tensor $\mathbf{\Phi}_\tau^t(\mathbf{x}_\tau)$. The vector $\hat{\mathbf{r}}(t)$ denotes the rotated position of $\mathbf{r}_\tau$ under the evolving axis of rotation of $\mathbf{\Phi}_\tau^t(\mathbf{x}_\tau)$.

This rotation angle is independent of the frame of reference and can be computed incrementally over any two times τ and t. Consequently, $\psi_{t_0}^t(\mathbf{x}_0)$ gives an appealing alternative to the polar rotation angle $\Theta_{t_0}^t(\mathbf{x}_0)$ for extracting a local rigid body rotation in the flow in a self-consistent manner. The intrinsic dynamic rotation angle also creates a direct connection with vorticity and hence is more connected with the fluid-mechanical intuition for local rotation in the flow.

At the same time, $\psi_{t_0}^t(\mathbf{x}_0)$ depends on the choice of the reference fluid mass $D(t)$ with respect to which the mean vorticity $\bar{\omega}(s)$ is computed. In practice, one chooses $D(t)$ to be the full domain over which the velocity field is known. This arguably gives the best-

https://doi.org/10.1017/9781009225199.003 Published online by Cambridge University Press

informed assessment for the deviation of local rotation from the overall rotation of the fluid, as represented by the integrand in Eq. (2.132).

2.4 Are the Eulerian and Lagrangian Approaches Equivalent?

The Lagrangian and Eulerian descriptions of fluid motion are sometimes portrayed as equivalent alternatives, with each defined in a different frame. For steady flows, or more generally, directionally steady velocity fields of the form (2.51), this statement is correct: an instantaneous snapshot of the velocity field holds all information about the past and future of all material trajectories. Specifically, streamlines coincide with particle trajectories.

Another rare direct connection between Eulerian and Lagrangian evolution is known for steady incompressible inviscid flows. In such a flow, any Lagrangian instability manifested by a positive Lyapunov exponent (such as the instability caused by a saddle-type stagnation point or by chaotic trajectories) implies that the flow, as a whole, is unstable. Specifically, typical small, incompressible and inviscid perturbations to the velocity field will grow in time at a rate that is at least as fast as the rate of the Lagrangian instability within the flow (see Appendix A.3).

For general unsteady flows, however, the only connection between the Eulerian and Lagrangian descriptions is that the Lagrangian particle trajectories are solutions of the differential equation (2.17), whose right-hand side is the Eulerian velocity field. This differential equation has solutions that generally differ vastly from those of the differential equation (2.3) for streamlines. To illustrate this, we consider the 2D unsteady velocity field

$$\mathbf{v}(\mathbf{x},t) = \begin{pmatrix} -\sin ct & \cos ct + a \\ \cos ct - a & \sin ct \end{pmatrix} \begin{pmatrix} x \\ y \end{pmatrix} - b \begin{pmatrix} y^2 - x^2 \\ 2xy \end{pmatrix}, \tag{2.133}$$

with the parameters a, b, $c \in \mathbb{R}$ (see Pedergnana et al., 2020). A direct substitution shows that the velocity field (2.133) is a solution of the 2D version of the Navier–Stokes equation (2.67) for any value of the viscosity, given that the Laplacian of Eq. (2.133) vanishes. This velocity field has simple spatiotemporal behavior as it depends periodically on time and quadratically on space. In the left subplot of Fig. 2.23, two broadly used Eulerian diagnostics, the instantaneous streamlines and the Okubo–Weiss elliptic region (see §3.7.1) are shown for Eq. (2.133).

This picture is qualitatively similar for all other initial times $t_0 \neq 0$ as well, except that the features rotate around the origin as t_0 is varied. Therefore, the two Eulerian diagnostics suggest the presence of a vortical feature in the center of the flow. In the right subplot of the same figure, the same Eulerian analysis is shown, but now with the result of some key Lagrangian flow structures superimposed. Specifically, the stable and unstable manifolds[18] of the fixed point at the origin are shown, indicating chaotic mixing due to the presence of a homoclinic tangle (see §4.1.1). This implies the complete lack of a closed, vortical region surrounding the origin in the Lagrangian dynamics. Therefore, the two Eulerian diagnostics provide a false positive for a coherent vortex that would inhibit mixing. Their prediction would be inconsistent with any dye or particle experiment carried out on this flow.

[18] These manifolds can be constructed numerically by observing that the flow linearized at the origin becomes steady in an appropriate rotating frame (see Pedergnana et al., 2020), and hence the tangent spaces of stable and unstable manifolds at the origin are known explicitly for all times.

https://doi.org/10.1017/9781009225199.003 Published online by Cambridge University Press

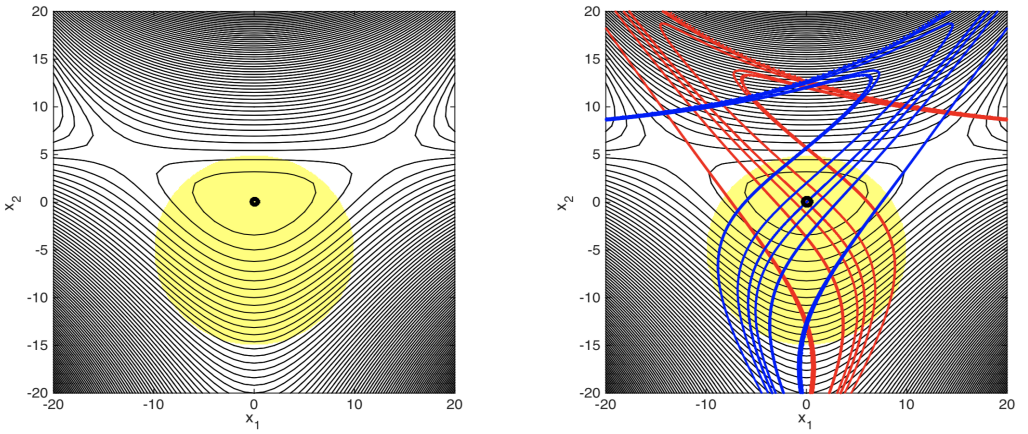

Figure 2.23 Eulerian and Lagrangian features in the Navier–Stokes velocity field (2.133) for $a = 2$, $b = 0.1$ and $c = -4$ at time $t = 0$. (Left) Streamlines (black) and Okubo–Weiss elliptic region (yellow), with the latter marking points where vorticity dominates the rate-of-strain eigenvalues in norm. (Right) Same but with the stable and unstable manifolds of the Poincaré map $\mathbf{P}_0 = \mathbf{F}_0^{\pi/4}$ (see §4.1.1) superimposed.

As a second example, Fig. 2.24 shows the results of similar analyses for the parameter configuration for a different parameter configuration in the Navier–Stokes velocity field (2.133) (see Pedergnana et al., 2020). In this case, the complete absence of closed streamlines and Okubo–Weiss elliptic domains in the region shown suggests hyperbolic (stretching) behavior, whereas the Lagrangian dynamics is, in fact, elliptic (vortical) around the origin. Therefore, the two Eulerian diagnostics, provide a false negative for a coherent vortex, which again would be in contradiction with the results of flow visualization experiments carried out on this velocity field.

The 2D Navier–Stokes velocity-field family (2.133), depending on the planar variable $\mathbf{x} = (x, y)$, also generates an exact solution family for the full, 3D Navier–Stokes equation (2.67) (see Majda and Bertozzi, 2002). Indeed, if we partition the 3D spatial variable as $(\mathbf{x}, z)$ and seek a corresponding 3D Navier–Stokes velocity field $(\mathbf{v}(\mathbf{x}, t), w(\mathbf{x}, t))$ and pressure field $p(\mathbf{x}, t)$, then substitution of this trial solution into Eq. (2.67) with $\mathbf{g} = \mathbf{0}$ yields the advection–diffusion equation

$$w_t + \boldsymbol{\nabla} w \cdot \mathbf{v} = \nu \Delta w \tag{2.134}$$

for the unknown vertical velocity component $w(\mathbf{x}, t)$. This equation will have a unique solution $w(\mathbf{x}, t)$ for any initial vertical-velocity distribution $w(\mathbf{x}, t_0) = w_0(\mathbf{x})$, with the simplest solution being $w(\mathbf{x}, t) \equiv 0$. The latter choice extends our 2D conclusions above about discrepancies between the Eulerian and the experimentally observable Lagrangian flow descriptions to 3D flows.

One might still argue that instantaneous Eulerian features, such as streamlines, vorticity and strain are more relevant for the physics of fluids than Lagrangian particle behavior. This view, however, is in sharp contrast with the considerations involved in the heuristic derivations of common Eulerian diagnostics (see §3.7.1), which all start out by seeking

https://doi.org/10.1017/9781009225199.003 Published online by Cambridge University Press

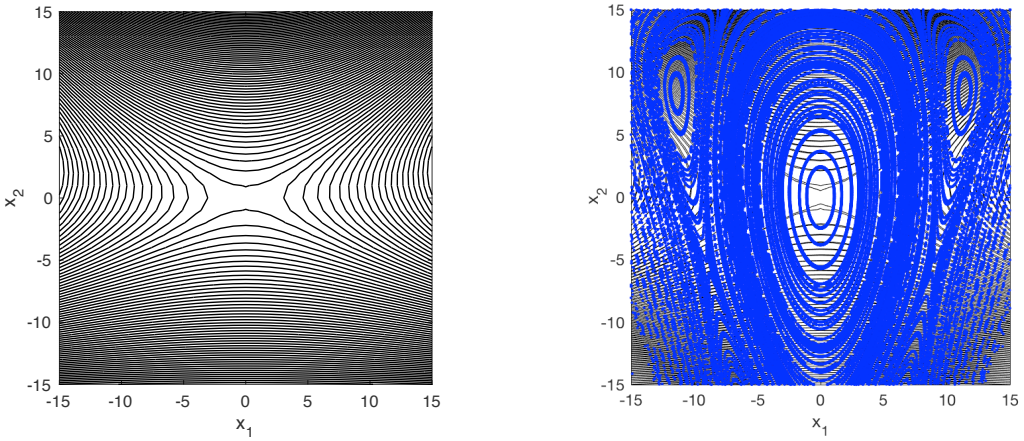

Figure 2.24 Eulerian and Lagrangian features in the Navier–Stokes velocity field (2.133) for $a = 0.5$, $b = -0.015$ and $c = -4$ at time $t = 0$. (Left) Streamlines and Okubo–Weiss hyperbolic region (white background), with the latter marking points where the rate-of-strain eigenvalues dominate the vorticity in norm. (Right) Same but with iterations of a grid of initial conditions under the Poincaré map $\mathbf{P}_0 = \mathbf{F}_0^{\pi/4}$ (see §4.1.1) superimposed in blue.

to classify regions of qualitatively different *fluid particle motion*. All these derivations are then invariably faced with the insurmountable challenge of classifying solution behavior in nonlinear, non-autonomous differential equations without solving for trajectories of these equations. It is at that point that the derivations depart from the originally stated objective and replace Lagrangian considerations with instantaneous Eulerian reasoning.

The assessment from Eulerian diagnostics applied to the example velocity field (2.133) also depends on the frame of the observer. In contrast, the assessment of Lagrangian flow topology provided by the Poincaré map is independent of the frame and hence is intrinsic to the flow. This discrepancy highlights the importance of the *principle of objectivity* (or frame-indifference) as a fundamental requirement for self-consistent flow structure detection, as proposed in the 1970s by Drouot (1976), Drouot and Lucius (1976) and Lugt (1979). We will elaborate on this principle and its implications in Chapter 3.

2.5 Summary and Outlook

In this chapter, we have surveyed the basic Eulerian and Lagrangian concepts along with results that we will be using throughout this book to describe transport barriers and coherent structures. On the Eulerian side, we have recalled the notion of the velocity field $\mathbf{v}(\mathbf{x}, t)$, its gradient $\nabla\mathbf{v}$ and the unique decomposition of $\nabla\mathbf{v}$ as a sum of the symmetric rate-of-strain tensor $\mathbf{S}$ and the skew-symmetric spin tensor $\mathbf{W}$. We have also reviewed the notions of stagnation points, streamlines and streamsurfaces from a geometric perspective, with an emphasis on their structurally stable types.

Among the Lagrangian tools discussed, the central notion has been the flow map, $\mathbf{F}_{t_0}^{t}$, which enables a geometric treatment of sets of fluid particle trajectories (pathlines) in the

https://doi.org/10.1017/9781009225199.003 Published online by Cambridge University Press

phase space of the dynamical system generated by a velocity field $\mathbf{v}(\mathbf{x}, t)$. Material lines, material curves and fixed points can then all be viewed as invariant manifolds of this map. Spatially or temporally recurrent flows are often easier to study under stroboscopic samplings of $\mathbf{F}_{t_0}^{t}$, which has led us to discuss temporal and spatial Poincaré maps.

We have reviewed detailed properties of the deformation gradient, $\nabla \mathbf{F}_{t_0}^{t}$, including various decompositions of this two-point tensor that seek to identify different components of material deformation. The deformation gradient is also key to the definition of the various strain tensors we have introduced to describe large deformations in fluid flows. We have also surveyed available global mathematical predictions for volume- or mass-conserving flows confined to compact domains. These predictions include the repeated return of trajectories arbitrarily close to their initial positions (Poincaré's recurrence theorem) and the convergence of time-averages of observables to their spatial averages in perfectly mixing flows (Birkhoff's ergodic theorem). While neither of these theorems is applicable to particle motion in temporally aperiodic velocity fields, both theorems will be important in the study of transport barriers to steady and temporally recurrent flows in Chapter 4.

Our survey of Lagrangian results has focused entirely on deterministic flows, even though Lagrangian fluid mechanics has traditionally emphasized statistical methods. This tradition has been motivated by the complexity of turbulence, which continues to inspire stochastic flow models and their statistical analysis (see, e.g., Dryden et al., 1941; Monin and Yaglom, 2007; Sabelfeld and Simonov, 2012). In contrast, this book focuses on flows known as specific velocity data sets, which in turn generate specific deterministic (albeit often complex), finite-time, nonautonomous dynamical systems for fluid motion.[19] For this reason, we have collected here the most important tools that arise in the data-driven global analysis of structurally stable invariant sets of nonautonomous dynamical systems. In Chapter 8, we will also discuss barriers for stochastic transport, but will find that such barriers can still be fully captured from the data-driven analysis of the deterministic component of the velocity field under small stochasticity.

[19] We will study structurally stable transport barriers in such a realization of a fluid flow, as those barriers are guaranteed to persist in close enough realizations of the same flow.

https://doi.org/10.1017/9781009225199.003 Published online by Cambridge University Press